Land surface model photosynthesis and parameter calibration for boreal sites with adaptive population importance sampler

Jarmo Mäkelä[1], Jürgen Knauer[2], Mika Aurela[1], Andrew Black[3], Martin Heimann[2], Hideki Kobayashi[4], Annalea Lohila[1,5], Ivan Mammarella[5], Hank Margolis[6], Tiina Markkanen[1], Jouni Susiluoto[1], Tea Thum[2], Toni Viskari[1], Sönke Zaehle[2], and Tuula Aalto[1]

[1]Finnish Meteorological Institute, P.O. Box 503, 00101 Helsinki, Finland
[2]Max Planck Institute for Biogeochemistry, 07745 Jena, Germany
[3]Department of Applied Biology, University of British Columbia, Canada
[4]Institute of Arctic Climate and Environment Change Research, Japan Agency for Marine-Earth Science and Technology, Japan
[5]Institute for Atmospheric and Earth System Research / Physics, P.O. Box 48, Faculty of Science, FI-00014 University of Helsinki, Finland
[6]Department of Forest Sciences, University of Quebec, Canada

Correspondence: Jarmo Mäkelä (jarmo.makela@fmi.fi)

Abstract. We calibrated the JSBACH model with six different stomatal conductance formulations using measurements from 10 FLUXNET coniferous evergreen sites in the Boreal zone. The parameter posterior distributions were generated by adaptive population importance sampler and the optimal values by a simple stochastic optimisation algorithm. The observations used to constrain the model are evapotranspiration (ET) and gross primary production (GPP). We identified the key parameters in the
5 calibration process. These parameters control the soil moisture stress function and the overall rate of carbon fixation.

We were able to improve the coefficient of determination and the model bias with all stomatal conductance formulations. There was no clear candidate for the best stomatal conductance model, although certain versions produced better estimates depending on the examined variable (ET, GPP) and the used metric. We were also able to significantly enhance the model behaviour during a drought event in a Finnish Scots pine forest site.

10 The JSBACH model was also modified to use a delayed effect of temperature for photosynthetic activity. This modification enabled the model to correctly time and replicate the springtime increase in GPP (and ET) for conifers throughout the measurements sites used in this study.

1 Introduction

Plants exchange carbon dioxide (CO_2) and water (H_2O) with atmosphere. Sufficient soil water, irradiance and adequate temper-
15 ature are required to maintain the exchange rate during the growing season. Disturbances in these conditions such as drought, cold temperature or low radiation cause the plants to respond to the environmental stress via stomatal closure and the drawdown of photosynthesis and transpiration (Lagergren and Lindroth, 2002; Mäkelä et al., 2004; Gao et al., 2017). The capability of

plants to recover from such events depends on species and their adaptation to site conditions (Kozlowski and Pallardy, 2002). Stress is part of the normal annual cycle of the plants, but occasionally it may exceed the limits of recovery.

Soil water deficit and high water vapour pressure deficit can result in suppressed plant transpiration (Bréda et al., 1993; Kropp et al., 2017) and boreal forests occasionally suffer from soil drought (Muukkonen et al., 2015; Gao et al., 2016). Globally soil
5 drought has been recognised as one of the main limiting factors for plant photosynthesis (Nemani et al., 2003). The recovery of photosynthetic capacity in spring has been connected to temperature history, and to frequency of severe night frosts (Bergh et al., 1998; Bergh and Linder, 1999) reversing the development. Understanding, and correctly modelling, these phenomena are especially important to boreal forests (Bonan, 2008) under changing environmental conditions.

Ecosystem and land surface models, describing the plant photosynthesis, transpiration and soil hydrology related processes,
10 usually include descriptions and parametrisations for various stress effects. These parameters often lack a theoretical foundation (Gao et al., 2002; Medlyn et al., 2011) and descriptions of vegetation drought response and phenology have been recognized to need better representations (Richardson et al., 2012; Powell et al., 2013; Xu et al., 2013; Medlyn et al., 2016). These deficiencies restrict the model's predictive capability under changing environmental conditions, and call for specific parametrisations for different plant types and vegetation zones.

15 The stomatal conductance models describe the pathway of CO_2 and water through the leaf stomata by an electric circuit analogy (Nobel, 1999). The variations in stomatal opening and mesophyll structure are interpreted as resistances to the water flow and the process is idealised via generalised parameterisation. The stomatal conductance models mainly differ in their choice of variable driving the stomatal closure and their performance has been recently assessed in modelling by e.g. Egea et al. (2011); Knauer et al. (2015); Franks et al. (2018). However, it can be hypothesised that the choice of the stomatal conductance model
20 affects the ecosystem model parameters more broadly than just those directly related to the stomatal conductance formulations. A holistic assessment of the performance of the stomatal conductance models together with parameter optimisation has been missing.

In this study we apply the land-surface model JSBACH for 10 boreal coniferous evergreen forest eddy covariance sites to examine the performance of different stomatal conductance models, and their effect on calibrated parameters related to
25 photosynthesis, phenology and hydrology. We will assess the inter-site variability and focus on a specific drought period at one site. We will provide an assessment of the robustness of the calibration of parameters together with different stomatal conductance descriptions. We utilise the adaptive population importance sampler to sample the full parameter space with the different stomatal conductance formulations and to locate different modes of the target (peaks of high probability).

2   Materials and methods

30 The site level measurements, required by the model as input variables, are air temperature, air pressure, precipitation, humidity, wind speed and CO_2 concentration as well as short- and longwave and potential shortwave radiation. Additionally evapotranspiration (ET) and gross primary production (GPP), derived from the eddy covariance (EC) measurements, are used to constrain and evaluate the model.

2.1 Sites and measurements

We use data from 10 FLUXNET (doi:10.17616/R36K9X) sites characterised as coniferous evergreen forests. Site descriptions with appropriate references are gathered in Table 1. The site level half-hourly measurements were quality checked and gap-filled when needed to produce continuous half-hourly and daily time series. The gap-filled and low quality (based on FLUXNET

5   data quality flags) measurements were masked and the daily aggregates accepted as part of the calibration process if at least 60% of values between 4:00 and 20:00 for that day were unmasked.

Based on the quality and quantity of their respective measurements, the sites were divided into calibration and validation sites. Essentially, if we have enough data (at least eight years and without too many gaps), the site is used for both calibration and validation purposes (with measurements separated into successive time periods), otherwise the site is used only for valida-

10   tion. The FLUXNET datasets were missing both the long- and shortwave radiation for the two Russian sites, Fyodorkovskoye (RU-Fyo) and Zotino (RU-Zot). These were generated from ERA Interim data. The soil types of all of these sites can mostly be identified as mineral soils with varying sand, clay and peat contents. Fyodorovskoye and Poker Flat (US-Prr) are natural peatlands and Lettosuo (FI-Let) is a drained peatland site.

The measurement error in the EC flux data can be separated into systematic and random errors. The main systematic errors

15   (density fluctuations, high-frequency losses, calibration issues) are taken into account as part of the post-processing of the data, and the random errors tend to dominate the uncertainty of the instantaneous fluxes. The random error is often assumed Gaussian but can be more accurately approximated by a symmetric exponential distribution (Richardson et al., 2006). It increases linearly with the magnitude of the flux, with a standard deviation typically less than 20% of the flux (Richardson et al., 2008; Rannik et al., 2016). Our treatment of the measurement (and model) error is explained in section 2.9.

Table 1. Descriptions for the sites used in this study sorted by their FLUXNET identifier. The first six sites are used for both calibration and validation purposes, and the following four for validation only. The reported elevation is in meters above sea level, LAI is the one-sided leaf area index and the average stand age is in years, along with average annual precipitation (P) in mm and temperature (T) in degrees Celsius.

Site id	lat	lon	elev.	dom. species	LAI	age	P	T	years	reference
CA-Obs	53.99	-105.12	629	*Picea mariana*	3.8	135	406	0.8	1999–2006	Chen et al. (2006)
CA-Qfo	49.69	-74.34	382	*Picea mariana*	3.7	112	962	-0.4	2003–2010	Chen et al. (2006)
FI-Hyy	61.85	24.29	180	*Pinus sylvestris*	3.5	45	709	2.9	1999–2006	Kolari et al. (2009)
FI-Ken	67.99	24.24	337	*Picea abies*	2.1	100	484	0.4	2003–2010	Aurela et al. (2015)
FI-Sod	67.36	26.64	179	*Pinus sylvestris*	1.7	150	527	-0.4	2001–2008	Thum et al. (2007)
RU-Fyo	56.45	32.90	265	*Picea abies*	4.5	200	711	3.9	2002–2009	Launiainen et al. (2016)
CA-Ojp	53.92	-104.69	579	*Pinus banksiana*	2.6	100	431	0.1	2004–2006	Chen et al. (2006)
FI-Let	60.64	23.96	119	*Pinus sylvestris*	6.0	40	627	4.6	2010–2012	Launiainen et al. (2016)
RU-Zot	60.80	89.35	121	*Pinus sylvestris*	1.5	215	493	-3.3	2002–2004	Kelliher et al. (1998)
US-Prr	65.12	-147.49	210	*Picea mariana*	0.7	72	275	-2.0	2011–2013	Ikawa et al. (2015)

2.2   The JSBACH model version 3.10

JSBACH (Kaminski et al., 2013) is a process-based ecosystem model and the land surface component of the Earth System model of Max Planck Institute for Meteorology (MPI-ESM). We ran JSBACH offline using an observational meteorological data set to force the model. Implications of this one-way coupling with the atmosphere include lack of feedback from the

5   surface energy balance to the atmosphere, i.e. latent and sensible heat fluxes and surface thermal radiation do not directly affect prescribed air temperature or humidity. Similarly the feedback of surface to the vertical transfer coefficients within the atmospheric surface layer is missing as the wind speed that drives mixing is prescribed. Furthermore, since we use site level data (each site is represented as a single grid point), the grid resolution does not affect the results (Tesfa et al., 2014; Singh et al., 2015).

10   We focus only on the most essential parts of JSBACH relating to our work. A more complete model description with details on e.g. soil heat transfer, water balance and coupling to the atmosphere can be found in Roeckner et al. (2003), whereas Raddatz et al. (2007) provides a more descriptive synopsis on land-surface interactions, Reick et al. (2013) supplements both with land cover change processes and Hagemann and Stacke (2015) introduces soil hydrological mechanisms within a multilayer scheme applying five layers.

15   In JSBACH the land surface is a fractional structure where the land grid-cells are divided into tiles representing the most prevalent vegetation classes called plant functional types (PFTs) within each grid cell (Reick et al., 2013). The grid cell is first divided into bare soil and vegetative area which is furthermore fractionally divided into PFTs. In our site level simulations, the model was set to use only one PFT, coniferous evergreen trees. The seasonal development of leaf area index (LAI) for the trees is regulated by air temperature and soil moisture with a single limiting value (for all sites) for the maximum of LAI. This

20   maximum value was fixed and the site-specific fractions of vegetative area were adjusted to reproduce the measured site level LAI.

The predictions of phenology are produced by the Logistic Growth Phenology (LoGro-P) model of JSBACH (Böttcher et al., 2016). Photosynthesis is described by the biochemical photosynthesis model (Farquhar et al., 1980). Following Kattge et al. (2009) we set the maximum electron transport rate (J_{max}) at 25 degrees Celsius to 1.9 times the maximum carboxylation rate

25   ($V_{C,max}$), which is in line with e.g. Leuning (2002); Ueyama et al. (2016). The photosynthetic rate is dependent on the used stomatal conductance formulation, introduced in chapter 2.3. Radiation absorption is estimated by a two stream approximation within a three-layer canopy (Sellers, 1985). Especially in the sparse canopies, the radiation absorption is affected by clumping of the leaves which is here taken into account according to the formulation by Knorr (1997).

Parameters detailing site-specific soil properties, such as soil porosity and field capacity, were derived from FLUXNET

30   datasets and the references in Table 1. We approximated the soil compositions and generated these properties following Hagemann and Stacke (2015).

2.3 Modifications to the JSBACH model

All parameters of interest, presented in Table 2, were extracted from the JSBACH model code to an external file. The default parameter values are those used in the model and, in the case where we have introduced the parameters to the model, they are a synthesis of literature values. Most of the parameter ranges were adapted from our previous work on similar topic (Mäkelä et al., 2016), but they were also evenly sampled and adjusted keeping the setup of our simulations in mind. The parameter grouping was done to enhance optimisation and the mechanism is explained in chapter 2.6. Group I consists of parameters most directly affecting photosynthesis, group II parameters are intimately involved with soil moisture and group III are the logistic growth phenology (LoGro-P) model parameters. The equations governed by these parameters are presented in Appendix A.

Table 2. Descriptions of model parameters with default values, range and references to equations in the manuscript or in the appendixes. Parameters in the same group were calibrated simultaneously.

Parameter	def	range	Units	Group	Description	Eq.
$V_{C,max}$	62.5	[40,65]	$\diamond$	I	Farquhar model maximum carboxylation rate at 25°C of the enzyme Rubisco (coupled with maximum electron transport rate at 25°C with a factor of 1.9) [$\diamond = \mu$ mol(CO$_2$) m^{-2} s^{-1}].	A2
α	0.28	[0.26,0.32]	-	I	Farquhar model efficiency for photon capture at 25°C.	A4
τ	10.0	[5,15]	days	I	Adjustment period length in acclimation of photosynthesis.	1
c_b	5.0	[4,7]	-	I	Multiplier in momentum and heat stability functions (Louis, 1979).	-
f_{C3}	0.87	[0.7,0.95]	-	I	Ratio of C3-plant internal/external CO$_2$ concentration.	A3
q	0.0	[0,1]	-	I	Exponential scaling of water stress in reducing photosynthesis.	A1
g_0	0.001	[1E-5,5E-3]	∇	I	Residual stomatal conductance [$\nabla =$ mol m^{-2} s^{-1}].	B3
g_1	-	-	-	I	Slope of the stomatal conductance function. Values in Table 3.	B3
θ_{dr}	0.9	[0.5,0.95]	-	II	Volumetric soil water content above which fast drainage occurs.	A6
θ_{hum}	0.5	[0.2,0.8]	-	II	Fraction depicting relative surface humidity based on soil dryness.	A9
θ_{pwp}	0.35	[0.15,0.4]	-	II	Volumetric soil moisture content at permanent wilting point.	2
θ_{tsp}	0.75	[0.25,0.8]	-	II	Value of volumetric soil moisture content above which transpiration is unaffected by soil moisture stress (β); and $0.9\theta_{tsp} \geq \theta_{pwp}$.	2
p_{int}	0.25	[0.15,0.35]	-	II	Fraction of precipitation intercepted by the canopy.	A5
s_{sm}	5.9E-3	[1E-4,0.1]	m	II	Depth for correction of surface temperature for snow melt.	-
w_{skin}	2.0E-4	[1E-5,5E-3]	m	II	Maximum water content of the skin reservoir of bare soil.	-
C_{decay}	13.0	[5,25]	days	III	LoGro-P: memory loss parameter for chill days.	A12
S_{min}	10.0	[5,30]	$^{\circ}$C days	III	LoGro-P: minimum value of critical heat sum.	A12
S_{range}	150.0	[100,300]	$^{\circ}$C days	III	LoGro-P: maximal range of critical heat sum.	A12
T_{alt}	4.0	[2,10]	$^{\circ}$C	III	LoGro-P: cutoff in alternating temperature.	A10
T_{ps}	10.0	[3,25]	$^{\circ}$C	III	LoGro-P: memory loss parameter for pseudo soil temperature.	A14

Start of the growing season in the JSBACH model is defined by a "spring event", in the LoGro phenology model (appendix A3), that induces leaf growth. The phenology model calculates a sum of ambient temperature (heatsum) since last autumn that is above the cutoff value T_{alt}, presented in Eq. (A10). It also calculates a variable threshold, defined in (A12), for the heatsum sum to reach. The threshold decreases based on the number of days the ambient temperature is below T_{alt}, whereas the heatsum

5   increases. When the heatsum reaches the threshold, the plant leaves are free to grow.

However, coniferous evergreen trees do not shed all of their leaves for winter and are therefore in readiness for the following spring. The start of the photosynthetically active season in the model has been observed to occur too early in the Boreal region by e.g Böttcher et al. (2016). To correct this behaviour i.e. to restrain the respiration and photosynthesis of conifers, we utilise a delayed effect of temperature for photosynthetic activity, introduced by Mäkelä et al. (2004). To calculate the reduction, we

10   must first define the state of photosynthetic acclimation that Mäkelä et al. (2004, p.371) present as: "an aggregated measure of the state of those physiological processes of the leaves that determine the current photosynthetic capacity at any moment".

The state of acclimation (S) is calculated from air temperature (T) with a delay prescribed by parameter τ (this is similar to the calculation of T_S in appendix A14). S is then inserted into sigmoidal relation Eq. (1) to calculate a factor γ, a formulation that is adapted here from Kolari et al. (2007). Finally γ is used to reduce the photosynthetic efficiency in Eq. (A1). $T_{1/2}$ denotes

15   the inflection point where γ reaches half of γ_{max}, b is the curvature of the function and $\gamma = 1$ when $S \geq 10$.

$$\frac{dS}{dt} = \frac{T - S}{\tau}, \qquad \gamma = \frac{\gamma_{max}}{1 + e^{b(S - T_{1/2})}} \tag{1}$$

The JSBACH model was also modified to include altogether six different stomatal conductance formulations following Knauer et al. (2015). These formulations include the pre-existing Baseline and Bethy versions as well as the Ball-Berry model and three of its variants. Model information is gathered in Table 3 for easy referencing and the detailed formulations are given

20   in appendix B. The limits of the slope of the conductance formulation parameter (g_1) were set to reflect commonly observed values from physiological measurements (Egea et al., 2011). Likely due to human error, the bounds for g_1^{USO} were not adjusted accordingly.

Table 3. Stomatal conductance models with default values and range for g_1 and references to equations in Appendix B as well as related articles. The ⋆ symbol indicates the Ball-Berry model and its variants.

Stomatal conductance model	short	g_1	range	references	
Baseline	Base	-	-	B1	Knorr (1997)
Biosphere-Energy-Transport-Hydrology	Bethy	-	-	B2	Knorr (2000)
⋆ Ball-Berry	BB	9.0	[4,10]	B3	Ball et al. (1987)
⋆ Leuning	Leu	8.0	[6,10]	B3	Leuning (1995)
⋆ Friend and Kiang	F&K	9.5	[7,11]	B3	Friend and Kiang (2005)
⋆ Unified stomatal optimisation	USO	2.0	[1.5,3.5]	B3	Medlyn et al. (2011)

All of the stomatal conductance models contain an empirical water stress factor β, which reduces stomatal conductance as a function of volumetric soil water content (θ).

$$\beta = \begin{cases} 1, & \theta \geq \theta_{tsp} \\ \frac{\theta - \theta_{pwp}}{\theta_{tsp} - \theta_{pwp}}, & \theta_{pwp} < \theta < \theta_{tsp} \\ 0, & \theta \leq \theta_{pwp} \end{cases} \tag{2}$$

In the original JSBACH formulation, the Baseline version, the stomatal conductance (g_s) is first resolved for unstressed canopy and then scaled by β. The Bethy approach assumes that transpiration is either limited by atmospheric demand or water supply. In cases when water supply is not the limiting factor, the calculations are similar to the Baseline version. In all of the empirical Ball-Berry variants, the stomatal conductance can be written as $g_s = g_0 + c\beta g_1$. The residual conductance (g_0) and the slope of the function (g_1) are both formulation specific parameters as well as factor c, that incorporates net photosynthesis and effects of atmospheric humidity and CO_2 concentration. The parameters g_0 and g_1 are part of our sampling and optimisation processes (group I in Table 2 when applicable).

2.4 Parameter estimation

The usual problem in parameter estimation is to infer a parameter distribution or a (optimal) set of parameter values $\mathbf{x} \in \mathcal{X} \subset \mathbb{R}^n$ (such as the maximum a posteriori or MAP estimate) with a given set of observations or measurements $\mathbf{y} \in \mathbf{R}^d$ on some model. Generally the parameter probability density function (pdf), with the given measurements, $p(\mathbf{x}|\mathbf{y})$ cannot be directly accessed. However, it can be represented as a product of the parameter prior distribution $p(\mathbf{x})$ and the likelihood (or data distribution) $p(\mathbf{y}|\mathbf{x})$ of the measurements with the given parameters. Using Bayes' rule on conditional probability we can write the posterior pdf as:

$$p(\mathbf{x}|\mathbf{y}) = \frac{p(\mathbf{x}, \mathbf{y})}{p(\mathbf{y})} = \frac{p(\mathbf{x})p(\mathbf{y}|\mathbf{x})}{p(\mathbf{y})} = \frac{g(\mathbf{x})l(\mathbf{y}|\mathbf{x})}{Z(\mathbf{y})} \tag{3}$$

In the last step we have substituted to the same notation as in Martino et al. (2015). We describe the modelling setup with the observation equation $\mathbf{y} = M(\mathbf{z}, \mathbf{x}) + \mathbf{e}$. The model M produces estimates of the observations $\mathbf{y}$ from the model state $\mathbf{z}$ (that includes the driving data) using the current parameter values $\mathbf{x}$. The residuals $\mathbf{e}$ are gathered by the likelihood function $l(\mathbf{y}|\mathbf{x})$ (formulated in section 2.9), which depicts how we handle the model–data mismatch.

The denominator $Z(\mathbf{y})$ is called the partition function (or model evidence) and it is often disregarded as it does not depend on the drawn sample $\mathbf{x}$ and can thus be viewed as a constant. Many Markov chain Monte Carlo (MCMC) methods simply state that $p(\mathbf{x}|\mathbf{y}) \propto g(\mathbf{x})l(\mathbf{y}|\mathbf{x}) = \pi(\mathbf{x})$ and leave it at that, however Z can be useful in e.g. model selection. On a more general setting (since APIS is able to handle these), the expected value of any measurable function $f(\mathbf{x})$, with respect to the pdf $\pi(\mathbf{x})$, can be expressed as:

$$I = E[f(\mathbf{X})] = \frac{1}{Z} \int_{\mathcal{X}} f(\mathbf{x})\pi(\mathbf{x})d\mathbf{x}, \qquad Z = \int_{\mathcal{X}} \pi(\mathbf{x})d\mathbf{x} \tag{4}$$

In the simulations at hand, the function f is the identity operator, but for completeness sake we will write it out as a function.

2.5 Adaptive population importance sampler

The adaptive population importance sampler (APIS) (Martino et al., 2015) is a Monte Carlo (MC) method for efficiently computing integrals involving complicated multidimensional target probability density functions, such as Eq. (4). This method utilises a population of importance samplers (IS) to jointly estimate the target pdf $\pi(\mathbf{x})$ and the normalising constant Z by a

5   deterministic mixture approach (Veach and Guibas, 1995; Owen and Yi, 2000). Normally during this process only the location parameters of the IS proposals are adapted, but we also adapt the shape parameters. The APIS is able to use different or a mixture of normalised proposals densities, but we utilise truncated Gaussian proposals with diagonal covariance matrices.

A basic IS estimator draws N samples $\mathbf{x}_i, i \in \{1,...,N\}$ from a single proposal distribution $q(\mathbf{x})$. The estimator then calculates importance weights (w_i) for each sample and approximates the integral Eq. (4) as:

10   $$w_i = \frac{\pi(\mathbf{x}_i)}{q(\mathbf{x}_i)}, \qquad I = E[f(\mathbf{X})] \approx \frac{\sum_i w_i f(\mathbf{x}_i)}{\sum_i w_i} \tag{5}$$

This evaluation is rarely sufficient if the target is even slightly complicated. One classical way of tackling this problem is to join multiple IS estimators together. The simplest approach is to calculate the weights for each of these estimators separately and to normalise the result by the combined sum of all weights. The basic IS estimator, and by extensions the simply joint estimator, is driven by the discrepancy between the target and proposal densities. This feature leaves the estimator susceptible

15   to "bad" proposals.

The APIS suppresses the bad proposals by utilising the deterministic mixture approach (Veach and Guibas, 1995; Owen and Yi, 2000) presented in Eq. (6), where each proposal $q_j, j \in \{1,...,M\}$ is evaluated at all the drawn samples and weighed by the amount of samples drawn (N_j) from that proposal. This is equivalent to joining the normalised proposal densities together and evaluating the joint pdf.

20   $$w_{ij} = \frac{\pi(\mathbf{x}_{ij})}{\sum_j \left(\frac{N_j}{\sum_k N_k} \right) q_j(\mathbf{x}_{ij})} \qquad \Rightarrow \qquad I \approx \frac{1}{\sum_{ij} w_{ij}} \sum_{ij} f(\mathbf{x}_{ij}) w_{ij}, \qquad Z \approx \frac{\sum_{ij} w_{ij}}{\sum_j N_j} \tag{6}$$

In the APIS adaptation, the estimates for I and Z in Eq. (6) are iteratively adjusted and the location and shape parameters of the proposal distributions are updated. In our experiments, this is done at predefined intervals, after drawing $N = 50$ samples from each of our $M = 40$ proposals. The location $(\boldsymbol{\mu}_j)$ and shape $(\mathbf{C}_j)$ parameters for each proposal are updated using only samples drawn from that proposal and weights calculated by the basic IS estimator:

25   $$\boldsymbol{\mu}_j = \frac{\sum_i w_i \mathbf{x}_i}{\sum_i w_i}, \qquad \mathbf{C}_j = \frac{\sum_i w_i (\mathbf{x}_i - \boldsymbol{\mu}_j)(\mathbf{x}_i - \boldsymbol{\mu}_j)^T}{\sum_i w_i} \tag{7}$$

The final configuration of the APIS proposal means $(\boldsymbol{\mu}_j)$ is expected to be around all the modes of the target, the parameter posterior distribution $p(\mathbf{x}|\mathbf{y})$. The shape parameter adaptation is not normally part of the APIS procedure, but we have adapted the diagonal elements of the proposal covariance matrix using the self-normalising AMIS estimators by Cornuet et al. (2012). The new covariance is the weighted mean of the previous covariance and the new estimate.

30   There is one final note to be made about the sampling process. The first sample of each proposal is always fixed as the proposal mean. This requirement is due to our desire to reduce the needed computational time – we generate the model starting

state (chapter 2.7) only for the proposal means and use the same state for the other 49 samples from that proposal. To mitigate the discrepancy this induces, we slightly scale the importance weights based on the distance of the corresponding sample to the mean of the proposal. This scaling is only used in the adaptation of location and shape parameters.

2.6 Parameter optimisation

5 The APIS algorithm is a rather robust method meant for examining the full target probability distribution and e.g. locating the modes of the target distribution. In order to find the optimal set of parameters (within a reasonably short amount of iterations), we utilise a simple custom stochastic optimiser, with starting points set at the modes of the target. This optimiser is run after the APIS calibration.

Our optimiser is a simple random sampler amplified by the "velocity" of the last jump (the idea is similar to Hamiltonian 10 or Hybrid Monte Carlo by Duane et al. (1987)). We draw a set of samples from a small Gaussian proposal distribution in the vicinity of the current best estimate and calculate the cost function for the samples. Whenever a better point is found (smaller cost function), we jump to that (update the mean of the proposal distribution). The "velocity" of the jump (for us merely distance of change in each parameter) is then added to the new mean (with a maximal limit of one standard deviation in the proposal distribution), but it is reduced and eventually removed if a better sample is not found.

15 The covariance matrix of the proposal distribution is recalculated at predefined intervals (for all parameters). Additionally the samples are first drawn from the full parameter space, in the next step they are drawn only from group I in Table 2 (the rest are kept at their current optimal values), followed by groups II and III and then back to the full parameter space. When the number of parameters is reduced, we are more likely to find a better set of parameter values. We have kept the parameters mostly affecting the same processes in the same group, but some dependencies may not be apparent and hence it is also important to 20 draw samples from the full parameter space.

2.7 Simulations

The initial state of the JSBACH model can be generated from predefined values of state variables that usually describe empty initial storage pools or the model can be restarted from a file describing the state of some previous run. Depending on the area of interest, a model spin-up may be required to bring the model into a steady state. In our simulations some of the more 25 slowly changing variables (e.g. soil water content and LAI) need to be equilibrated, so a spin-up of 20 years is used. This can be achieved by running the model over a set of measurements multiple times, each time restarting from the final state of the previous run.

The calibration period consists of the first five years given for the calibration sites in Table 1. The spin-up is achieved by looping over these years multiple times and then saving the state of the model at the end of the run. The actual calibration is 30 started from the beginning of the calibration period, using the previously saved state variables. To reduce any bias this induces, the first year in the calibration run is removed from the cost function calculations.

In APIS simulations the spin-up is generated each time the proposal means are adapted. With the optimisation algorithm, run after the APIS simulations, the spin-up is generated for each sample. The validation run for the six calibration sites continues

directly after the calibration run (so the spin-up is created, calibration period run and followed by the validation run when applicable). The spin-ups for the four validation sites in Table 1 are similarly generated and the first year of the period discarded.

During the summer 2006, the Hyytiälä (FI-Hyy) measurement site suffered from a severe drought (Gao et al., 2017). These events are difficult for models to capture, hence we have also calibrated the model parameters using Hyytiälä measurements

5   from 2006. The spin-up was the same as for the calibration period, but at the end of the spin-up the model was run forward to the start of the year 2006. Only values between the 190–260th day of the year (DOY) in 2006 were used in constraining the model.

2.8   Simulation analysis

We have utilised a Gaussian kernel density estimation (KDE) to produce distributions from generated samples. In practice,

10   KDE places a Gaussian distribution centred at each sample and the constructed composite distribution is an estimate of the underlying actual distribution. The bandwidth for the distributions is calculated using the Scott's rule (Scott, 2004): the data covariance matrix is multiplied by a factor $n^{\frac{-1}{d+4}}$, where n is the number of data points and d is the number of dimensions.

The effectiveness of each parameter was calculated from the final state of each optimisation process. This was done by first setting all parameters to their optimised values. Then we (evenly) sampled each parameter separately from their range of

15   acceptable values and calculated the corresponding cost functions. For each parameter the maximum difference in these cost function values (and the optimised value) was recorded. The parameters (within each optimisation) were then ordered by these numbers (with highest difference meaning highest effectiveness) and separated into three groups with "high", "average" or "low" effectiveness value.

We report the slope of the regression line (b) and the coefficient of determination (r^2), between the observations (y_i) and the

20   model output (x_i). The slope of the regression line is highly indicative of the model bias (difference of the expected values of the observations and the model). Hence we interpret the bias directly from b (in our results the regression lines pass near origin so the differences this induces are negligible).

$$b = \frac{\sum_i (x_i - \overline{x_i})(y_i - \overline{y_i})}{\sum_i (y_i - \overline{y_i})^2}, \qquad r^2 = 1 - \frac{\sum_i (x_i - y_i)^2}{\sum_i (y_i - \overline{y_i})^2} \tag{8}$$

2.9   Cost function

25   The cost function (9) in our simulations is based on the mean squared error (MSE) estimates of gross primary production (GPP) and evapotranspiration (ET). The residual of each variable is divided by the mean of observations, as has been previously done successfully by e.g. Mäkelä et al. (2016); Knauer et al. (2015); Groenendijk et al. (2010); Trudinger et al. (2007). We make use of this approach since we needed to balance two series of different magnitudes (ET and GPP).

Optimally we would scale the residuals by a covariance vector, combining the model and observational errors, but unfor-

30   tunately this is not possible. The model error is unknown as is the (pointwise) observation error. We could use a general type of error estimate (such as that of 20% of the flux value) for the observations, but would have to include a minimal site and instrumentation dependent precision. In this study, the full error is treated as Gaussian white noise. The cost function is calcu-

lated for each site separately, with the gap-filled and low-quality points removed (leaving N_{ET} and N_{GPP} points), and then averaged over the sites.

$$cf_1 = \overbrace{\frac{1}{N_{ET}} \sum \left(\frac{ET_{mod} - ET_{obs}}{\overline{ET_{obs}}} \right)^2}^{\text{NMSE}_{ET}} + \overbrace{\frac{1}{N_{GPP}} \sum \left(\frac{GPP_{mod} - GPP_{obs}}{\overline{GPP_{obs}}} \right)^2}^{\text{NMSE}_{GPP}} \qquad (9)$$

We also use a modified version of this cost function, where the normalised mean squared error estimates (NMSE) are

5 weighted by factors based on coefficients of determination (r^2) defined in Eq. (8). This latter cost function is only used during the separate drought period optimisation for Hyytiälä.

$$cf_2 = (1 - r_{ET}^2)\text{NMSE}_{ET} + (1 - r_{GPP}^2)\text{NMSE}_{GPP} \qquad (10)$$

3 Results and discussion

We will begin this section by examining the performance of the APIS algorithm and the parameters themselves, followed

10 by stomatal conductance model specific site level results and lastly an examination of the Hyytiälä drought event in 2006. For convenience sake, and to simplify sentences, we will equate the name of the stomatal conductance model to that of the JSBACH model utilising that conductance formulation.

The evolution of the APIS algorithmic process is presented in Fig. 1 for three parameters from the calibration of the Bethy model. The parameters were chosen to highlight different levels of identifiability for the algorithm (with the given cost func-

15 tion). The first parameter (f_{C3}) is an example of a well identifiable situation, where the algorithm quickly locates the area of high probability. The second parameter (θ_{dr}) is also identifiable but the speed of convergence is diminished. The last example (C_{decay}) represents situations when the algorithm is unable to constrain the parameter. This can happen when the signal from a parameter (the effect the parameter would have on the values of the cost function) is too weak (when compared to the signals from other sources) for the algorithm to capture. We have included parameter posterior distributions (at 20 iterations) as

20 supplement (S1).

We used 40 proposal distributions and drew 50 samples from each, accumulating to 2 000 samples from the 18–21 (depending on the stomatal conductance model) dimensional parameter space at a time. After 20 such iterations (40 000 samples) the algorithm produced reasonably stable distributions for most parameters. The APIS sampling process did not reveal any multimodal distributions and thus provided suitable initial conditions for the optimisation. The results of the optimisation process

25 are gathered in Table 4. Some of the parameters have converged near their limiting values, which can reflect deficiencies in the model structure or the preset parameter ranges. Convergence to a liming value can also be a problem in model calibration, but in this expirement the algorithms were able to cope with the situation as APIS located the area of high probability and the optimiser located the maxima. The different parameter effectiveness levels reported in Table 4 can be roughly equated to the identifiability situations in Fig. 1. The effectiveness levels are highly situational (e.g. they depend on the sampling limits set

30 for each parameter) and merely reflect the parameter identifiability in the APIS process.

In many other studies, where the aim has been to optimise land system model parameters, the optimisation is based on estimating the gradient of the cost function: Knorr et al. (2010) for JSBACH, Kuppel et al. (2012); Peylin et al. (2016) for ORCHIDEE and Raoult and Luke (2016) for JULES. The gradient-based methods are faster than MCMC methods as they strongly steer the sampling process to reach a minima of the cost function. This approach also enables a more indefinite setting

5 of parameter ranges when compared to methods that sample the full parameter space. However, they are prone to get stuck in a local minima, especially when the dimensionality of the parameter space increases. Lately similar parameter estimations have also been done for CLM by Post et al. (2017) using the DREAM$_{(zs)}$ (MCMC) algorithm with multiple chains, and for JULES by Iwema et al. (2017) with the BORG algorithm that employs multiple optimisation algorithms simultaneously. The DREAM algorithm is fully iterative, which limits the number of parallel processes to the number of parallel chains in use (when we do

10 not account for the possibility of the model parallelisation that can be substantial). The applicability of the BORG algorithm is dependent on the algorithms in use and the expertise of the user (to choose the right algorithms etc.).

APIS can be run iteratively as presented by Martino et al. (2015) but also in parallel, since all samples (prior to each adaptation) can be drawn and estimated simultaneously. This latter feature is useful to decrease the amount of real time required to run the algorithm (and the model) when computer resources are not the limiting factor. In the iterative mode, automatic

15 stopping rules can be easily implemented to indicate when additional samples are not required to improve the estimates. The APIS algorithm samples the full parameter space (as do other MCMC methods), is able to utilise a mixture of parameter prior distributions and can estimate complicated multidimensional probability distributions. These aspects make APIS an attractive alternative to the other sampling and optimisation methods.

3.1 Optimised parameters

20 A curious reader might have noticed that the last two parameters in Table 4 have not been introduced. These are empirical parameters explicit for the Friend and Kiang (Friend and Kiang, 2005) stomatal conductance formulation in B3. We calibrated the model without these parameters and the resulting cost function (9) values were poor when compared to the other formulations. At that point, these parameters were included in the optimisation process. This increases the degrees of freedom for the Friend and Kiang model by two and therefore may give it an advantage when compared to the other Ball-Berry type formulations,

25 which has to be considered in the interpretation of the results.

Before we delve into Table 4, we would like to draw the reader's attention to the exponential scaling factor q in Eq. (A1) of the β-function (2) for reducing photosynthesis. This is an experimental parameter that has been revealed to be ineffective in our optimisation. However, ineffectiveness does not equal irrelevance – in the case of q, the situation arises as the effective range of the β-function has been reduced by lowering θ_{tsp}. The actual soil moisture in our simulations is rarely below this

30 fraction, so q is optimised with a very limited number of datapoints and therefore the values presented for it in Table 4 can be are unreliable and even unrealistic.

The LoGro phenology parameters, that affect the timing of the spring and autumn events, are expected to contribute only little to the cost function. The coniferous evergeen trees do not shed all their leaves for winter and therefore the timing of

Table 4. Parameter default and optimised values for the calibration period with corresponding cost function value. The values written in boldface were the most effective and the italic values the least effective for the given experiment. Also presented are the fixed parameter values for the drought period optimisation (explained in section 3.3), with opt referring to the use of the corresponding optimised value from this table.

Parameter	def	Base	Bethy	BB	Leu	F&K	USO	dry set
$V_{C,max}$	62.5	48.4	57.1	55.4	49.7	50.8	**50.5**	52.0
α	0.28	0.318	0.318	0.319	0.317	0.319	0.318	0.318
τ	10.0	14.6	15.0	14.8	14.9	14.7	14.8	14.8
c_b	5.0	5.4	4.1	6.7	*4.4*	*4.3*	4.6	5.0
f_{C3}	0.87	**0.75**	**0.83**	-	-	-	-	Table 6
q	0.0	*0.03*	0.94	*0.62*	*0.60*	*0.82*	*0.65*	Table 6
θ_{dr}	0.9	0.86	*0.65*	0.88	0.83	0.8	*0.90*	0.85
θ_{hum}	0.5	**0.2**	**0.2**	**0.21**	**0.2**	**0.2**	**0.2**	Table 6
θ_{pwp}	0.35	**0.16**	**0.15**	**0.17**	**0.15**	**0.16**	**0.15**	Table 6
θ_{tsp}	0.75	**0.31**	**0.35**	**0.3**	**0.31**	**0.32**	**0.33**	Table 6
p_{int}	0.25	0.35	0.35	0.35	0.35	0.35	0.35	0.35
s_m	5.9E-3	0.099	*0.094*	*0.097*	*0.098*	0.097	*0.078*	0.097
w_{skin}	2.0E-4	**3.7E-4**	**3.1E-4**	**3.5E-4**	**3.6E-4**	**3.3E-4**	**3.2E-4**	3.4E-4
C_{decay}	13.0	*17.0*	22.2	23.3	23.3	24.9	*13.9*	opt
S_{min}	10.0	*29.2*	26.3	*10.7*	6.3	*26.1*	6.3	opt
S_{range}	150	*247*	176	*162*	*157*	*202*	*223*	opt
T_{alt}	4.0	2.0	2.8	5.8	8.2	2.5	8.3	opt
T_{ps}	10.0	*18.6*	24.4	3.8	3.2	15.0	3.1	opt
g_0	1.0E-3	-	-	4.7E-3	4.7E-3	4.4E-3	4.2E-3	Table 6
g_1	Table 3	-	-	**9.9**	**8.8**	10.9	1.6	Table 6
a	2.8	-	-	-	-	3.2	-	opt
b	80	-	-	-	-	**71**	-	opt
cf_1		0.571	0.531	0.521	0.529	0.518	0.528	

the bud burst is not as critical as for e.g. deciduous trees. Additionally the state of acclimation parameter τ also affects the vegetation active period and likely dominates the phenology parameters.

There is an overall agreement on the values of the most prevalent parameters between the models. Most notably the permanent wilting point (θ_{pwp}) and the point above which transpiration is unaffected by soil moisture stress (θ_{tsp}) have been

5   significantly lowered. This change to model parameters can be perceived at least in two different ways. Either the boreal forests are not generally limited by soil moisture stress (except in the case of extreme drought) or the water retention capa-

bilities of the soil (in the model) have been systematically overestimated. We will focus more thoroughly on these and the parameters, that were part of the drought period optimisation, in section 3.3.

Some of the parameters in this study have been calibrated before by e.g. Kattge et al. (2009); Knorr et al. (2010). Our approach differs from these as we required the model to reproduce the site level maximum of LAI by fixing the limiting value

5 and adjusting the site-specific fractions of bare soil and vegetative area. In contrast e.g. Knorr et al. (2010) found the structural limit for (all-sided) LAI to be 4.2, which is considerably lower than the measured LAI for many of the sites in Table 1. Our approach directly scales the vegetative area, so it also scales GPP and e.g. the amount of rain available for plants (as rain is directed to bare soil and vegetative area). This means that the parameter values should not be directly compared without taking the different paradigms into account. However our optimised $V_{C,max}$ values are in-between 62.5 reported by Kattge et al.

10 (2009) and 29.3 by Knorr et al. (2010) and are in line with the yearly cycle presented by Ueyama et al. (2016).

Mäkelä et al. (2004) used a linear dependency of photosynthetic efficiency to the state of acclimation, and reported 13.75 days to be the best fit for the adjustment period length (τ). Kolari et al. (2007) utilised a sigmoidal relation and reported the value of 8 days, but noted that the range of values resulting in a good fit was large (5–10.4 days). Linkosalo et al. (2014) came to a similar conclusion when they encounter a near-flat distribution for τ in the range of 1–12 days. In our simulations

15 τ exhibits slightly larger optimal values, which is most likely due to the model adapting to the multi-site calibration (as sites have different characteristics, a longer acclimation period accounts these variation better).

3.2 Site level results

We present the average annual cycles for the validation period and for all sites in Fig. 2 using the Bethy formulation. We chose to present the Bethy results since this stomatal conductance formulation is part of the standard model and the results are

20 slightly more in line with the Ball-Berry variants than those with the Baseline model. Similar figures for the other stomatal conductance models are added as supplements (S2–S6) – the actual images are very much alike. The relevant values of the slope of the regression line (b) and the coefficient of determination (r^2) from all of these images have been gathered in Table 5. These indicators have been calculated using all corresponding values regardless of quality. The sites are in the same order as in Table 1 with the six calibration sites first, followed by the four sites used only for validation.

25 On a first glance, the optimisation has improved the model results in Fig. 2 for all of the calibration sites and at least for half of the validation sites. The improvement in the timing of the springtime increase in GPP is apparent. The GPP increase now occurs later in springtime and this same effect is also reflected in transpiration, and consequently in ET. This correction in the ET values can lead to an increase in model bias as is the case with Sodankylä (FI-Sod), where the too low autumn values were previously compensated by too high springtime values with the default parametrisation. This increase in bias should not

30 be viewed as a fault in the optimisation as the model was previously mitigating an erroneous behaviour (too low autumn ET) with another (too high springtime ET).

The correlation coefficients for ET and GPP have improved for every site and the GPP bias has diminished for all calibration sites – the two validation sites where GPP bias has increased are Poker Flat (US-Prr) and Zotino (RU-Zot). These two sites have the lowest site level LAI values and the site understory likely contributes to significant amount of GPP – approximately

Table 5. Slope of the regression line (b) and the coefficient of determination (r^2) for the different stomatal conductance formulations during the validation period with the optimised parameters. We have written the best values of b and r^2 in boldface for each site and italicised the abbreviations of the separate validation sites.

| | Evapotranspiration (ET) | | | | | | | | | | | |
| | b | | | | | | r^2 | | | | | |
Site	Base	Bethy	BB	Leu	F&K	USO	Base	Bethy	BB	Leu	F&K	USO
CA-Obs	0.91	0.9	**0.91**	0.86	0.81	0.76	0.86	**0.88**	0.87	0.87	0.87	0.86
CA-Qfo	0.96	0.98	**0.99**	0.92	0.89	0.83	0.84	**0.85**	0.84	0.84	0.84	0.83
FI-Hyy	0.97	1.1	1.1	0.95	**0.98**	0.79	0.85	**0.88**	0.88	0.87	0.88	0.83
FI-Ken	0.54	**0.64**	0.62	0.56	0.58	0.48	0.69	0.71	**0.72**	0.7	0.71	0.67
FI-Sod	0.64	0.73	**0.74**	0.63	0.64	0.56	0.76	**0.8**	0.78	0.77	0.79	0.74
RU-Fyo	0.98	1.0	1.0	0.98	**0.99**	0.85	0.83	0.85	0.84	0.84	**0.85**	0.84
CA-Ojp	0.8	**0.84**	0.84	0.75	0.72	0.67	0.8	**0.81**	0.8	0.81	0.8	0.79
FI-Let	1.1	0.98	1.1	1.0	**1.0**	0.94	0.7	0.69	0.7	0.71	**0.71**	0.7
RU-Zot	0.49	**0.56**	0.56	0.47	0.46	0.41	0.67	**0.72**	0.71	0.68	0.69	0.64
US-Prr	0.38	0.37	**0.42**	0.35	0.33	0.35	0.7	0.72	**0.73**	0.68	0.66	0.66
best values	0	3	4	0	3	0	0	6	2	0	2	0
	Gross primary production (GPP)											
	b						r^2					
Site	Base	Bethy	BB	Leu	F&K	USO	Base	Bethy	BB	Leu	F&K	USO
CA-Obs	**0.83**	0.77	0.82	0.81	0.81	0.77	0.93	0.95	0.94	0.94	**0.95**	0.95
CA-Qfo	0.97	0.95	**0.98**	0.96	0.96	0.9	0.92	0.93	0.92	0.93	**0.94**	0.93
FI-Hyy	1.0	**1.0**	1.0	1.0	1.1	0.98	0.97	0.97	0.97	0.98	**0.98**	0.98
FI-Ken	0.9	0.97	**0.97**	0.93	0.95	0.9	0.96	0.95	0.95	0.97	0.97	**0.97**
FI-Sod	0.66	0.71	**0.71**	0.67	0.69	0.65	0.94	0.93	0.93	0.94	**0.95**	0.95
RU-Fyo	0.95	0.88	0.91	0.96	**0.98**	0.91	0.95	0.94	0.94	0.95	0.95	**0.96**
CA-Ojp	0.72	0.74	**0.75**	0.7	0.69	0.66	0.91	0.92	0.91	0.92	0.93	**0.93**
FI-Let	1.3	**0.99**	1.1	1.3	1.3	1.2	0.96	0.94	0.95	0.97	0.97	**0.97**
RU-Zot	0.42	**0.44**	0.44	0.42	0.42	0.4	0.93	0.92	0.92	0.94	**0.94**	0.94
US-Prr	0.2	**0.21**	0.21	0.2	0.19	0.19	0.79	0.78	0.77	0.79	**0.79**	0.79
best values	1	4	4	0	1	0	0	0	0	0	6	4

half of the CO_2 fluxes for Poker Flat are produced by the site understory (Ikawa et al., 2015). These factors alone do not seem sufficient in explaining the problems the model has with the Poker Flat site.

There are two further explanations for the less-than-perfect predictive skill seen. The first is our choice of adjusting the site-specific fractions of vegetative and bare soil areas to reproduce the measured site level maximum of LAI. This can affect the model behaviour especially for sites with very low (Zotino) or high (Lettosuo (FI-Let)) site level LAI as the adjustment linearly changes the proportions between vegetative area and bare soil. The second explanation is that there are also many parameters describing site-specific soil properties (such as porosity) that were not part of the optimisation and may be inaccurate. The latter may also be pronounced due to the changes in parameters affecting soil moisture.

There were no clear differences between sites dominated by pine or spruce. Neither did we notice any particular effect on the bias, MSE or correlation coefficient that could be explained by geographical location, stand age or annual precipitation or temperature. We optimised the model for individual (calibration) sites as well. Mostly this changed the values of parameters (such as $V_{C,max}$ and g_1) affecting the amplitude of the modelled fluxes. These parameters can be viewed to be more site-specific, a characteristics that is reduced in a multi-site calibration – the possibility of highly site-specific properties (and parameter values) can also explain the difficulties in reproducing the validation site observations. We are omitting these results as single-site optimisation can be viewed as overfitting the model and the results do not provide any additional insights.

We can compare the b and r^2 values with the various stomatal conductance models, reported in Table 5, but the overall differences are small. The r^2 values are reasonably good for both ET and GPP, even for the low LAI sites RU-Zot and US-Prr. The prominent bias in both variables for the low LAI sites is apparent here as well.

Similarly to the results by Knauer et al. (2015), there is no clear candidate for the best stomatal conductance formulation. The different metrics (b, r^2) and variables (ET, GPP) indicate better performance for some model versions, but these seem to be variable and metric specific. The best values tend to cluster to Bethy (13), F&K (12) and BB (12) formulations. However the results are not conclusive and for example we could have included the factor D_0 (that depicts stomatal sensitivity to changes in vapour pressure deficit D_s) in the optimisation, which would have likely improved the performance of the Leuning model.

3.3 Drought event in Hyytiälä

We have previously and unsuccessfully attempted to optimise the model (Mäkelä et al., 2016) for the Hyytiälä (FI-Hyy) exceptionally dry period (Gao et al., 2017). The drought was severe, leading e.g. to visible discolouration of needles. We focus now directly on the extended dry period (190–260th day of the year in 2006), during which the actual drought is mostly in effect between 215–240th DOY. The fixed parameter values during this optimisation are presented in Table 4. The maximum carboxylation rate $V_{C,max}$ was set to a value that enabled the full use of the dynamical range of q and it was an approximate mean of the optimised values. The LoGro phenology parameters and τ were fixed to their optimised values as they should not be affected during the drought. The other set values were compromises between the stomatal conductance formulations but these parameters should not take different values during the dry period. We note here that these decision were made from the modelling perspective and knowing the limitations of the models. It could be argued that i.e. the parameters $V_{C,max}$ and g_1 should fluctuate (Egea et al., 2011) during the drought but this does not fit in the model paradigm.

The other major change in the dry period optimisation was the use of the modified cost function (10). We have reduced the number of free parameters and essentially set the amplitude of GPP by fixing the parameter $V_{C,max}$. Hence we are more

interested in the correct timing of the change in GPP and ET fluxes, rather than the size of the actual change. The aim is to correctly reproduce the changes in the water use efficiency (WUE) of plants, which we interpret here as the pointwise ratio of (ecosystem level) GPP to ET. The normalised MSE values in cost function (10) ensure that the overall amplitude of the fluxes will remain satisfactory. The resulting optimised parameter values are presented in Table 6.

Table 6. Optimised parameter and corresponding cost function values with different stomatal conductance formulations for the extended dry period.

Parameter	def	Base	Bethy	BB	Leu	F&K	USO
f_{C3}	0.87	0.7	0.7	-	-	-	-
q	0.0	0.09	0.0	0.15	0.57	0.16	0.30
θ_{tsp}	0.75	0.57	0.46	0.48	0.44	0.45	0.41
θ_{pwp}	0.35	0.40	0.38	0.27	0.23	0.28	0.16
θ_{hum}	0.5	0.2	0.2	0.2	0.2	0.2	0.2
g_0	Table 3	-	-	4.9E-3	5.0E-3	3.8E-3	4.6E-3
g_1	Table 3	-	-	7.5	6.0	7.0	1.5
cf_2		0.42	0.44	0.39	0.41	0.41	0.41

5 We can now compare the parameter values in Table 6 to those in Table 4. The values of relative humidity parameter θ_{hum} and the residual stomatal conductance g_0 have remained nearly unchanged, but for the rest of the parameter we see wildly different results. Noticeably the USO optimisation only changes the value of θ_{tsp} and leaves the rest of the parameters almost untouched. This is probably partly due to our mistake of not adjusting the limits for g_1^{USO} properly before any model calibration. In this instance, the mistake works in our favour and we argue this because of two reasons. The drought period is very short and

10 any optimisation, with such limited data, can result in overfitting the model. Additionally, when the parameter values change radically under some special conditions, the fault can also be in the modelled processes. In the USO optimisation, these pitfalls have been avoided as only one of the parameter values has been changed (and the parameter in question merely shifts the upper bound for the β-function).

The most noteworthy is the behaviour of the slope of the stomatal conductance (g_1), where the previously high values (and

15 close to the upper bound) have been radically lowered. For two of the Ball-Berry variants (we disregard USO) it has reached the lower bound. However, we would argue that these g_1 parameters are close to their optimal values in this setting. The parameter g_1^{BB} has reached its optimal value and as the models in question are very similar and exhibit comparable results in Fig. 3, the optimal values are close. Overall, the decrease in the values of g_1 during the drought is expected as the plants close their stomata to minimise the loss of water by transpiration (Egea et al., 2011; Zhou et al., 2013).

20 The higher values of g_1 during the more general optimisation are better reflected by Franks et al. (2018), whereas the lower values during the drought are more in accordance with physiological observations by Egea et al. (2011). Likewise, Lin et al. (2015) found higher values for g_1 (both boreal area and gymnosperm trees) using the USO model. Our simulation setup for the

exponent q corresponds to the configuration 5 (C5) by Egea et al. (2011), with variables $q = q_B$ and fixed value $q_S = 1$ (we disregard the different values for θ_{tsp} and θ_{pwp}).

The site level estimates of (g_0 and) g_1 are sensitive to the stomatal conductance formulation but also e.g. to the general structure of the underlying model and the value of other parameters, such as maximum carboxylation rate ($V_{C,max}$). Wang
5 (1996) reported $g_1 = 3.78$ (control), using a Leuning model similar to ours, where $(1 + D_S/D_0)$ is replaced by D_S. (Thum et al., 2007) approximated $g_1^{BB} \approx 5$ for Sodankylä while estimating the variation in the values of $V_{C,max}$ and maximum rate of electron transport J_{max}. We would suggest that the limiting values θ_{pwp} and θ_{tsp} should be optimised or fixed before introducing additional tuning factors e.g. to mesophyll conductance or scaling the β in the stomatal conductance formulation (Egea et al., 2011).

10 The water stress in JSBACH is modelled via the soil moisture stress function (β). When the slope (g_1) of the stomatal conductance function ($g_s = g_0 + \beta g_1$) converges to the lower limit, the only viable option to further reduce carbon assimilation is to increase the β-function limits. The upper limit (θ_{tsp}) of this function is increased from the previously optimised values but is still far lower than the default value of 0.75 and the resulting values are fairly congruent (disregardin the Baseline formulation). The lower limit of the β-function (θ_{pwp}) exceeds the optimised value for all of the parametrisations and the
15 default value of 0.35 for the Baseline and Bethy formulations. The differences in the optimised values of θ_{pwp} can occur due to a larger impact, of the different stomatal conductance formulations to the accumulating soil water content, than assumed – this can be seen from the differences in the β-function values in Fig. 3. Additionally we could be overfitting the model, but the underlying model structure might also be lacking in e.g. by missing processes. Likely, all of these factor play a role.

The changes to modelled fluxes are visualised in Fig. 3. The Baseline, Bethy and USO formulations demonstrate a con-
20 siderable increase in the agreement in GPP between the model and observations when compared to the default setting or the previous more general optimisation. The GPP of other formulations has remained roughly the same as with the more generally optimised parameter values. The Baseline, Ball-Berry, Leuning, and to a lesser degree the Friend and Kiang formulations, now suffer from the too low ET values before the actual drought. The Bethy model has a too strong drawdown of both ET and GPP during the drought. The USO formulation results in the best fits for r^2 and b with the dry period optimisation and it makes full
25 use of the dynamical range of the β-function. Overall, the dry period optimisation was succesful for the USO model and to a lesser for the Bethy formulation as well – the results for the other variants are mixed and inconclusive.

We selected two of the stomatal conductance formulations, Bethy and USO, to examine the changes to the WUE of plants during the extended dry period. The highlighted observations in Fig. 4 show a clear path of development for the drought. Both observational colourings are similar (as are the β-functions) and depict first a linear decrease in both ET and GPP, followed by
30 a rapid decline in ET and a delayed decline in GPP. The recovery of plants from the drought can also be seen the colouring starts to turn lighter. The models depict a more linear response of GPP to ET as the drought develops, although with USO we can see a bit more similarities in the pattern of the values. The β-function, when optimised to the dry period, seems to be a reasonably good indicator of drought, when compared to the indicators presented by Gao et al. (2017).

Lastly, we inspected the ET and GPP cycles (not shown) for the whole validation period with both optimised parameter sets,
35 all stomatal conductance formulations and all calibration sites. The b and r^2 values for ET were better for all stomatal conduc-

tance formulations (except one) using the more generally optimised parameter set. There is some variation in the indicators for GPP, where approximately a third of the values (mostly r^2) are better with the dry period parameter set. These differences are mostly attributed to increased model bias (decreased b) that is explained by the lower values of g_1. Overall, the more general optimisation provided systematically better or comparable results to the dry period optimisation. The exception is the USO

5 formulation, which had an approximately 1:1 distribution of best values for both variables in-between the parameter sets.

4 Conclusions

The adaptive population importance sampler (APIS) is a recent method, capable of estimating complicated multidimensional probability distributions using a population of different proposal densities. The algorithm was able to produced reasonably stable estimates for most parameters quickly. Prior to calibrating the model, we adjusted the site-specific vegetative area frac-

10 tions to reproduce the measured site level maximum of LAI. This practical approach was successful, although we encountered difficulties in replicating ET and GPP fluxes for sites with low LAI. The model parameters were optimised simultaneously for all sites without any additional site level tuning. The parameters mostly affecting the optimisation processes were consistent for all stomatal conductance formulations.

The introduction of the S-function, to delay the start of the vegetation active season, has corrected the springtime increase

15 in GPP for conifers throughout the sites used in this study. The parameters θ_{tsp} and θ_{pwp}, that set the range for the soil moisture stress function β, were both systematically lowered and optimised to nearly identical values for all stomatal conductance models. This rendered the experimental parameter q nearly ineffective in the more general optimisation. The dry period optimisation increased the effective range of the β-function and the importance of q for the Ball-Berry type model. The Baseline and Bethy versions optimised q to be practically ineffective. Overall both optimisations strongly indicate that boreal forest

20 transpiration is not limited by soil moisture stress under normal conditions.

The optimisation improved the predictive skill of the model with all stomatal conductance formulations as was seen during the validation period. The Bethy, Ball-Berry and Friend and Kiang versions were the most compliant with the observations, although the differences between these and the other formulations were small. Most of the model versions had problems during the extended dry period. The unified stomatal optimisation model had the best b and r^2 values during the drought and utilised

25 the full range of the β-function. Additionally the optimised parameter values of the USO model for the dry period were the most coherent (of all stomatal conductance formulations) with those of the more general optimisation.

Code and data availability. The data required to calibrate and validate the model is part of the FLUXNET2015 dataset and it can be accessed through the FLUXNET database (doi:10.17616/R36K9X). The JSBACH model can be obtained from the Max Planck Institute for Meteorology, where it is available for scientific community (http://www.mpimet.mpg.de/en/science/models/license/). For any questions or

30 requests regarding the simulations data, we encourage you to contact the authors at jarmo.makela@fmi.fi.

Appendix A: Parametric equations within JSBACH

In this appendix we present the most relevant equations that are governed by the parameters in Table 2. The appendix is divided into sections that coincide with the parameter groups.

A1 Photosynthesis

5   The Farquhar model (Farquhar et al., 1980) is based on the observation that the assimilation rate in the chloroplast is limited either by the carboxylation rate (V_C), induced by the Rubisco enzyme, or the light-limited assimilation rate (J_E). The total rate of carbon fixation is reduced by the amount of dark respiration (R_d), resulting in net assimilation rate (A_n). The experimental scaling factor β^q (Egea et al., 2011) is based on soil moisture stress in Eq. (2), that takes effect ($\beta < 1$) when soil moisture is significantly reduced. This scaling is used by all stomatal conductance formulations. We have also introduced here in equation

10 form the actual reduction to photosynthesis by γ from the delay in the start of the vegetation active season in Eq. (1).

$$A_n = \beta^q(\min(\gamma V_C, J_E) - \gamma R_d) \tag{A1}$$

Oxygenation of the Rubisco molecule reduces the carboxylation rate, which is given as:

$$V_C = V_{C,max} \frac{C_i - \Gamma_\star}{C_i + K_C(1 + O_i/K_O)} \tag{A2}$$

Here C_i and O_i are the leaf internal CO_2 and O_2 concentrations, $\Gamma_\star$ is the photorespiratory CO_2 compensation point, K_C and

15 K_O are Michaelis-Menten constants parametrizing the dependence on CO_2 and O_2 concentrations. Furthermore, leaf internal CO_2 concentration depends on the external (ambient) concentration C_a (in the Baseline and Bethy formulations and unstressed conditions) by:

$$C_i = f_{C3} C_a \tag{A3}$$

Likewise, the light-limited assimilation rate can be expressed as a function on electron transport rate (J), which is a function

20 of radiation intensity (I) in the photosynthetically active band, the maximum electron transport rate (J_{max}) and the quantum efficiency for photon capture (α):

$$J_E = J(I) \frac{C_i - \Gamma_\star}{4(C_i + 2\Gamma_\star)}, \qquad J(I) = J_{max} \frac{\alpha I}{\sqrt{J_{max}^2 + \alpha^2 I^2}} \tag{A4}$$

A2 Soil water

In JSBACH the soil water budget is based on several reservoirs (e.g. skin, soil, bare soil, rain intercepted by canopy etc.) and

25 the different formulations are plentiful. We present here only the most crucial of these. Changes in soil water (θ_s, not to be confused with volumetric soil water content $\theta = \frac{\theta_s}{\theta_{fc}}$) due to rainfall ($R$), evapotranspiration ($ET$), snow melt ($M$), surface runoff ($R_s$) and drainage ($D$) are calculated with a geographically varying maximum field capacity (θ_{fc}).

$$\rho \frac{\partial \theta_s}{\partial t} = (1 - p_{int})R + ET + M - R_s - D \tag{A5}$$

The interception parameter (p_{int}) also affects the amount of water intercepted by vegetation and bare soil which further affects evaporation and transpiration. The skin reservoir is limited by w_{skin} and excess water is transferred to soil water. Likewise when the soil water content (θ) is greater than parameter θ_{dr}, the excess water is rapidly drained (in addition to the limited drainage below this threshold), where d, d_{min} and d_{max} are constant parameters:

$$D = d_{min}\theta + (d_{max} - d_{min})\left(\frac{\theta - \theta_{dr}}{1 - \theta_{dr}}\right)^d, \qquad \theta \geq \theta_{dr} \tag{A6}$$

Evaporation from wet surfaces (E_{ws}) depends on air density (ρ), specific humidity (q_a), saturation specific humidity (q_s) at surface temperature (T_s) and pressure (p_s) and aerodynamic resistance (R_a). The aerodynamic resistance depends on heat transfer coefficient (C_h) and horizontal velocity (v_h).

$$E_{ws} = \rho\frac{q_a - q_s(T_s, p_s)}{R_a}, \qquad R_a = C_h|v_h|^{-1} \tag{A7}$$

Transpiration from vegetation (T_v) is likewise formulated but additionally depends on the stomatal resistance of the canopy (R_c), which is an inverse of the stomatal conductance and as such, depends on which conductance model is used.

$$T_v = \rho\frac{q_a - q_s(T_s, p_s)}{R_a + R_c} \tag{A8}$$

Evaporation from dry bare soil (E_s) also has an added dependence on surface relative humidity (h_s) calculated from soil dryness:

$$E_s = \rho\frac{q_a - h_s q_s(T_s, p_s)}{R_a}, \qquad h_s = \max\left[\theta_{hum}(1 - \cos(\pi\theta)), \min\left(1, \frac{q_a}{q_s(T_s, p_s)}\right)\right] \tag{A9}$$

The total evapotranspiration is a weighted average of E_{ws}, T_v and E_s, where the weights are based on fill levels of reservoirs and the vegetative fraction of the grid cell.

A3 Logistic Growth Phenology (LoGro-P) model

The parameters from the LoGro-P are mainly used to determine the spring and autumn events for JSBACH. To determine the date of the spring event we first introduce a few additional variables, namely the heatsum $S_T(d)$, the number of chill days $C(d)$ and the critical heatsum $S_{crit}(d)$. $T(d)$ denotes the mean temperature at day d.

$$S_T(d) = \sum_{d'=d_0}^{d} \max(T(d') - T_{alt}, 0) \tag{A10}$$

Heatsum $S_T(d)$ cumulates the amount of "heat" above the parameter T_{alt} after the previous growing season. The actual starting date d_0 of the summation need not be known since it is enough to start the summation "reasonably late" after the last growth season.

$$C(d) = \sum_{d'=d_a}^{d} H\left(T_{alt} - T(d)\right) \tag{A11}$$

The number of chill days is calculated as the number of days when the mean temperature is below T_{alt}. Here $H()$ denotes the Heaviside step function and the summation starts at the day (d_a) of the last autumn event.

$$S_{crit}(d) = S_{min} + S_{range}e^{-C(d)/C_{decay}} \tag{A12}$$

The critical heatsum (S_{crit}) decreases as the number of chill days $C(d)$ increases, with an exponential memory loss parameter C_{decay}. The spring event happens when:

$$S_T(d) \geq S_{crit}(d) \tag{A13}$$

The autumn event requires the definition of one more variable, the (pseudo) soil temperature ($T_s(t)$), which at time t is calculated as an average air temperature (T) with an exponential memory loss (T_{ps}). The autumn event occurs when T_s falls below a certain threshold. In the equation N is the normalization constant and τ is the length of a time step.

$$T_s(t) = \frac{1}{N} \sum_{n=-\infty}^{t} T(n)e^{-(t-n)\frac{\tau}{T_{ps}}} \tag{A14}$$

Appendix B: Stomatal conductance formulations

In this appendix we present the stomatal conductance model formulations used in this study. In the original JSBACH formulation, the Baseline model (Knorr, 1997), the photosynthetic rate is resolved in two steps. First the stomatal conductance under conditions with no water stress is assumed to be controlled by photosynthetic activity (Schulze et al., 1994). Here the leaf internal CO_2 concentration is assumed to be a constant fraction ($C_{i,pot} = f_{C3}C_a$) of ambient CO_2 concentration (C_a). This allows for an explicit resolution of the photosynthesis (Knorr, 1997). Then the impact of soil water availability is accounted for by a soil moisture-dependent multiplier (β) that is identical for each canopy layer (Knorr, 1997).

$$g_{s,pot} = \frac{1.6A_{n,pot}}{C_a - C_{i,pot}} \qquad \Rightarrow \qquad g_s = \beta g_{s,pot} \tag{B1}$$

After accounting for soil water stress, the net assimilation rate (A_n) and intercellular CO_2 concentration are (C_i) are recalculated using g_s, and integrated over the leaf area index to produce canopy level estimates.

In the Bethy approach (Knorr, 2000), the unstressed canopy conductance ($G_{c,pot}$) is calculated similarly to the Baseline model, but potentially further limited by the water supply function of the maximum transpiration rate ($T_{supply} = \beta T_{max}$). T_{max} is a fixed and predefined upper limit for transpiration as in Knauer et al. (2015).

$$G_c = \begin{cases} G_{c,pot}\frac{T_{supply}}{T_{pot}}, & T_{pot} \geq T_{supply} \geq 0 \\ G_{c,pot}, & T_{pot} < T_{supply} \end{cases} \qquad , \qquad T_{pot} = \rho\frac{q_s - q_a}{1/G_a + 1/G_{c,pot}} \tag{B2}$$

The potential (unstressed) transpiration rate (T_{pot}) is a function of air density (ρ), saturation specific humidity (q_s) at given temperature and pressure, specific humidity (q_a), aerodynamic conductance (G_a) and unstressed canopy conductance ($G_{c,pot}$). After this scaling, the net assimilation rate and intercellular CO_2 concentration are recalculated as in the Baseline model.

The Ball-Berry variants relate the stomatal conductance (g_s) to empirically fitted parameters g_0 (mol m^{-2}s^{-1}) and g_1 (unitless, except for g_1^{USO} which has units of $\sqrt{\text{kPa}}$) that respectively represent the residual stomatal conductance and the slope of the function. The stomatal conductance is a function of the net assimilation rate (A_n), the water stress factor (β) and the atmospheric CO$_2$ concentration (C_a). The original Ball-Berry formulation (Ball et al., 1987) also depends on relative humidity

5 at leaf surface (h_s). In the Leuning model (Leuning, 1995), the CO$_2$ concentration is reduced by the CO$_2$ compensation point (Γ) as well as scaled by the vapour pressure deficit (D_s) and a constant (D_0) depicting the stomatal sensitivity to changes in D_s. The Friend and Kiang model (Friend and Kiang, 2005) adds an exponential dependency on the difference of specific (q) and saturation specific humidity (q_{sat}) with empirically fitted constants $a = 2.8$ and $b = 80$. The unified stomatal optimisation model (Medlyn et al., 2011) also adds a dependency to the vapour pressure deficit (D_s).

$$g_s^{BB} = g_0^{BB} + g_1^{BB}\beta\frac{A_n h_s}{C_a} \qquad\qquad g_s^{Leu} = g_0^{Leu} + g_1^{Leu}\beta\frac{A_n}{(C_a - \Gamma)(1 + D_s/D_0)} \qquad\text{(B3)}$$

$$g_s^{F\&K} = g_0^{F\&K} + g_1^{F\&K}\beta\frac{A_n a^{b(q_s - q_a)}}{C_a} \qquad\qquad g_s^{USO} = g_0^{USO} + 1.6\left(1 + \frac{g_1^{USO}\beta}{\sqrt{D_s}}\right)\frac{A_n}{C_a}$$

Author contributions. The experiments were planned by J. Mäkelä, T. Aalto, T. Markkanen and T. Thum. J. Mäkelä ran the simulations and prepared the manuscript with contributions from co-authors. J. Knauer originally implemented the Ball-Berry type stomatal conductance formulations into JSBACH under S. Zaehles supervision. J. Susiluoto maintained the framework for testing the algorithm. M. Aurela, A.

15 Black, M. Heimann, A. Lohila, I. Mammarella, H. Margolis and H. Kobayashi provided the site level observations required in this study. T. Aalto, T. Markkanen and T. Viskari extensively commented and revised the document.

Competing interests. The authors declare that they have no conflict of interest.

Acknowledgements. This work has been supported by Jenny and Antti Wihuri Foundation, the NordForsk Nordic Centre of Excellence under Grant no. 57001 (eSTICC) and the Academy of Finland under Grant no. 295874 (OPTICA), as well as Academy of Finland Centre

20 of Excellence under Grant no. 307331 and ICOS-Finland (project No. 281255) and EU-Life+ project MONIMET (LIFE12 ENV/FI000409). This work used eddy covariance data acquired and shared by the FLUXNET community, including these networks: AmeriFlux, AfriFlux, AsiaFlux, CarboAfrica, CarboEuropeIP, CarboItaly, CarboMont, ChinaFlux, Fluxnet-Canada, GreenGrass, ICOS, KoFlux, LBA, NECC, OzFlux-TERN, TCOS-Siberia, and USCCC. The FLUXNET eddy covariance data processing and harmonization was carried out by the ICOS Ecosystem Thematic Center, AmeriFlux Management Project and Fluxdata project of FLUXNET, with the support of CDIAC, and the

25 OzFlux, ChinaFlux and AsiaFlux offices.

References

Aurela, M., Lohila, A., Tuovinen, J., Hatakka, J., Penttilä, T., and Laurila, T.: Carbon dioxide and energy flux measurements in four northern-boreal ecosystems at Pallas, Boreal Environ. Res., 20, 455–473, http://www.borenv.net/BER/pdfs/ber20/ber20-455.pdf, 2015.

Ball, J., Woodrow, I., and Berry, J.: A Model Predicting Stomatal Conductance and its Contribution to the Control of Photosynthesis Under Different Environmental Conditions, Springer, Progress in Photosynthesis Research (edited by Biggins, J.), 221–224, https://doi.org/10.1007/978-94-017-0519-6_48, 1987.

Bergh, J. and Linder, S.: Effects of soil warming during spring on photosynthetic recovery in boreal Norway spruce stands, Glob. Change Biol., 5, 245–253, https://doi.org/10.1046/j.1365-2486.1999.00205.x, 1999.

Bergh, J., Mcmurtrie, R., and Linder, S.: Climatic factors controlling the productivity of Norway spruce: A model-based analysis, Forest Ecol. Manag., 110, 127–139, https://doi.org/10.1016/S0378-1127(98)00280-1, 1998.

Bonan, G.: Forests and Climate Change: Forcings, Feedbacks, and the Climate Benefits of Forests, Science, 320, 1444–1449, https://doi.org/10.1126/science.1155121, 2008.

Bréda, N., Cochard, H., Dreyer, E., and Granier, A.: Water transfer in a mature oak stand (Quercuspetraea): seasonal evolution and effects of a severe drought, Ca. J. Forest Res., 23, 1136–1143, https://doi.org/10.1139/x93-144, 1993.

Böttcher, K., Markkanen, T., Thum, T., Aalto, T., Aurela, M., Reick, C., Kolari, P., Arslan, A., and Pulliainen, J.: Evaluating Biosphere Model Estimates of the Start of the Vegetation Active Season in Boreal Forests by Satellite Observations, Remote Sensing, 8, 1–31, https://doi.org/10.3390/rs8070580, 2016.

Chen, J., Govind, A., Sonnentag, O., Zhang, Y., Barr, A., and Amiro, B.: Leaf area index measurements at Fluxnet Canada forest sites, Agr. Forest Meteorol., 140, 257–268, https://doi.org/10.1016/j.agrformet.2006.08.005, 2006.

Cornuet, J.-M., Marin, J.-M., Mira, A., and Robert, C.: Adaptive Multiple Importance Sampling, Scand. J. Stat., 39, 798–812, https://doi.org/10.1111/j.1467-9469.2011.00756.x, 2012.

Duane, S., Kennedy, A., Pendleton, B., and Roweth, D.: Hybrid Monte Carlo, Phys. Lett. B, 195, 216–222, https://doi.org/10.1016/0370-2693(87)91197-X, 1987.

Egea, G., Verhoef, A., and Vidale, P.: Towards an improved and more flexible representation of water stress in coupled photosynthesis–stomatal conductance models, Agric. Forest Meteorol., 151, 1370–1384, https://doi.org/10.1016/j.agrformet.2011.05.019, 2011.

Farquhar, G., Caemmerer von, S., and Berry, J.: A Biochemical Model of Photosynthetic CO_2 Assimilation in Leaves of C3 species, Planta, 149, 78–90, https://doi.org/10.1007/BF00386231, 1980.

Franks, P., G.B., B., J.A., B., D.L., L., N.M., H., N., H., and K.W., O.: Comparing optimal and empirical stomatal conductance models for application in Earth system models, Glob. Change Biol., 24, 5709–5723, https://doi.org/10.1111/gcb.14445, 2018.

Friend, A. and Kiang, N.: Land surface model development for the GISS GCM: Effects of improved canopy physiology on simulated climate, J. Climate, 18, 2883–2902, https://doi.org/10.1175/JCLI3425.1, 2005.

Gao, Q., Zhao, P., Zeng, X., Cai, X., and Shen, W.: A model of stomatal conductance to quantify the relationship between leaf transpiration, microclimate and soil water stress, Plant Cell Environ., 25, 1373–1381, https://doi.org/10.1046/j.1365-3040.2002.00926.x, 2002.

Gao, Y., Markkanen, T., Thum, T., Aurela, M., Lohila, A., Mammarella, I., Kämäräinen, M., Hagemann, S., and Aalto, T.: Assessing various drought indicators in representing summer drought in boreal forests in Finland, Hydrol. Earth Syst. Sci., 20, 175–191, https://doi.org/10.5194/hess-20-175-2016, 2016.

Gao, Y., Markkanen, T., Aurela, M., Mammarella, I., Thum, T., Tsuruta, A., Yang, H., and Aalto, T.: Response of water use efficiency to summer drought in boreal Scots pine forests in Finland, Biogeosciences, 14, 4409–4422, https://doi.org/10.5194/bg-14-4409-2017, 2017.

Groenendijk, M., Dolman, A., van der Molen, M., Leuning, R., Arneth, A., Delpierre, N., Gash, J., Lindroth, A., Richardson, A.D. Verbeeck, H., and Wohlfahrt, G.: Assessing parameter variability in a photosynthesis model within and between plant functional types using global Fluxnet eddy covariance data, Agric. Forest Meteorol., in press, 1–17, https://doi.org/10.1016/j.agrformet.2010.08.013, 2010.

Hagemann, S. and Stacke, T.: Impact of the soil hydrology scheme on simulated soil moisture memory, Clim. Dynam., 44, 1731–1750, https://doi.org/10.1007/s00382-014-2221-6, 2015.

Ikawa, H., Nakai, T., Busey, R., Kim, Y., Kobayashi, H., Nagai, S., Ueyama, M., Saito, K., Nagano, H., Suzuki, R., and Hinzman, L.: Understory CO_2, sensible heat, and latent heat fluxes in a black spruce forest in interior Alaska, Agr. Forest Meteorol., 214–215, 80–90, https://doi.org/10.1016/j.agrformet.2015.08.247, 2015.

Iwema, J., Rosolem, R., Rahman, M., Blyth, E., and Wagener, T.: Land surface model performance using cosmic-ray and point-scale soil moisture measurements for calibration, Hydrology and Earth System Sciences, 21, 2843–2861, https://doi.org/10.5194/hess-21-2843-2017, 2017.

Kaminski, T., Knorr, W., Schürmann, G., Scholze, M., Rayner, P., Zaehle, S., Blessing, S., Dorigo, W., Gayler, V., Giering, R., Gobron, N., Grant, J., Heimann, M., Hooker-Stroud, A., Houweling, S., Kato, T., Kattge, J., Kelley, D., Kemp, S., Koffi, E., Köstler, C., Mathieu, P.-P., Pinty, B., Reick, C., Rödenbeck, C., Schnur, R., Scipal, K., Sebald, C., Stacke, T., Terwisscha van Scheltinga, A., Vossbeck, M., Widmann, H., and Ziehn, T.: The BETHY/JSBACH Carbon Cycle Data Assimilation System: experiences and challenges, J. Geophys. Res-Biogeo., 118, 1414–1426, https://doi.org/10.1002/jgrg.20118, 2013.

Kattge, J., Knorr, W., Raddatz, T., and Wirth, C.: Quantifying photosynthetic capacity and its relationship to leaf nitrogen content for global-scale terrestrial biosphere models, Glob. Change Biol., 15, 976–991, https://doi.org/10.1111/j.1365-2486.2008.01744.x, 2009.

Kelliher, F., Lloyd, J., Arneth, A., Byers, J., McSeveny, T., Milukova, I., Grigoriev, S., Panfyorov, M., Sogatchev, A., Varlargin, A., Ziegler, W., Bauer, G., and E.-D., S.: Evaporation from a central Siberian pine forest, J. Hydrol., 205, 279–296, https://doi.org/10.1016/S0022-1694(98)00082-1, 1998.

Knauer, J., Werner, C., and Zaehle, A.: Evaluating stomatal models and their atmospheric drought response in a land surface scheme: A multibiome analysis, J. Geophys. Res-Biogeo., 120, 1894–1911, https://doi.org/10.1002/2015JG003114, 2015.

Knorr, W.: Satellite Remote Sensing and Modelling of the Global CO_2 Exchange of Land Vegetation: A Synthesis Study, Max-Planck-Institut für Meteorologie Examensarbeit, 49, 1894–1911, http://quest.bris.ac.uk/publications/knorr/thesis/thesis.html, 1997.

Knorr, W.: Annual and interannual CO2 exchanges of the terrestrial biosphere: process-based simulations and uncertainties, Global Ecol. Biogeogr., 9, 225–252, https://doi.org/10.1046/j.1365-2699.2000.00159.x, 2000.

Knorr, W., Kaminski, T., Scholze, M., Gobron, N., Pinty, B., Giering, R., and Mathieu, P.-P.: Carbon cycle data assimilation with a generic phenology model, J. Geophys. Res-Biogeo., 115, G04 017, https://doi.org/10.1029/2009JG001119, 2010.

Kolari, P., Lappalainen, H., Hänninen, H., and Hari, P.: Relationship between temperature and the seasonal course of photosynthesis in Scots pine at northern timberline and in southern boreal zone, Tellus B, 59, 542–552, https://doi.org/10.1111/j.1600-0889.2007.00262.x, 2007.

Kolari, P., Kulmala, L., Pumpanen, J., Launiainen, S., Ilvesniemi, H., Hari, P., and Nikinmaa, E.: CO_2 exchange and component CO_2 fluxes of a boreal Scots pine forest, Boreal Environ. Res., 14, 761–783, http://www.borenv.net/BER/pdfs/ber14/ber14-761.pdf, 2009.

Kozlowski, T. and Pallardy, S.: Acclimation and adaptive responses of woody plants to environmental stresses, Bot. Rev., 68, 270–334, https://doi.org/10.1663/0006-8101(2002)068[0270:AAAROW]2.0.CO;2, 2002.

Kropp, H., Loranty, M., Alexander, H., Berner, L., Natali, S., and Spawn, S.: Environmental constraints on transpiration and stomatal conductance in a Siberian Arctic boreal forest, Biogeosciences, 122, 761–783, https://doi.org/10.1002/2016JG003709, 2017.

Kuppel, S., Peylin, P., Chevallier, F., Bacour, C., Maignan, F., and Richardson, A.: Constraining a global ecosystem model with multi-site eddy-covariance data, Biogeosciences, 9, 3757–3776, https://doi.org/10.5194/bg-9-3757-2012, 2012.

5 Lagergren, F. and Lindroth, A.: Transpiration response to soil moisture in pine and spruce trees in Sweden, Agr. Forest Meteorol., 112, 67–85, https://doi.org/10.1016/S0168-1923(02)00060-6, 2002.

Launiainen, S., Katul, G., Kolari, P., Lindroth, A., Lohila, A., Aurela, M., Varlagin, A., Grelle, A., and Vesala, T.: Do the energy fluxes and surface conductance of boreal coniferous forests in Europe scale with leaf area?, Glob. Change Biol., 22, 4096–4113, https://doi.org/10.1111/gcb.13497, 2016.

10 Leuning, R.: A critical appraisal of a combined stomatal-photosynthesis model for C_3 plants, Plant Cell Environ., 18, 339–355, https://doi.org/10.1111/j.1365-3040.1995.tb00370.x, 1995.

Leuning, R.: Temperature dependence of two parameters in a photosynthesis model, Plant Cell Environ., 25, 1205–1210, https://doi.org/10.1046/j.1365-3040.2002.00898.x, 2002.

Lin, Y.-A., Medlyn, B., Duursma, R., Prentice, I., Wang, H., Baig, S., Eamus, D., de Dios, V., Mitchell, P., Ellsworth, D., de Beeck, M., Wallin, 15 G., Uddling, J., Tarvainen, L., Linderson, M.-L., Cernusak, L., Nippert, J., Ocheltree, T., Tissue, D., Martin-StPaul, N., Rogers, A., Warren, J., De Angelis, P., Hikosaka, K., Han, Q., Onoda, Y., Gimeno, T., Barton, C., Bennie, J., Bonal, D., Bosc, A., Löw, M., Macinins-Ng, C., Rey, A., Rowland, L., Setterfield, S., Tausz-Posch, S., Zaragoza-Castells, J., Broadmeadow, M., Drake, J., Freeman, M., Ghannoum, O., Hutley, L., Kelly, J., Kikuzawa, K., Kolari, P., Koyama, K., Limousin, J.-M., Meir, P., Lola da Costa, A., Mikkelsen, T., Salinas, N., and Sun, W.: Optimal stomatal behaviour around the world, Nat. Clim. Change, 5, 459–464, https://doi.org/10.1038/nclimate2550, 2015.

20 Linkosalo, T., Heikkinen, J., Pulkkinen, P., and Mäkipää, R.: Fluorescence measurements show stronger cold inhibition of photosynthetic light reactions in Scots pine compared to Norway spruce as well as during spring compared to autumn, Front. Plant Sci., 13, 1–8, https://doi.org/10.3389/fpls.2014.00264, 2014.

Louis, J.-F.: A parametric model of vertical eddy fluxes in the atmosphere, Bound.-Layer Meteor., 17, 187–202, 1979.

Mäkelä, A., Hari, P., Berninger, F., Hänninen, H., and Nikinmaa, E.: Acclimation of photosynthetic capacity in Scots pine to the annual cycle 25 of temperature, Tree Physiol., 24, 369–376, https://doi.org/10.1093/treephys/24.4.369, 2004.

Mäkelä, J., Susiluoto, J., Markkanen, T., Aurela, M., Järvinen, H., Mammarella, I., Hagemann, S., and Aalto, T.: Constraining ecosystem model with adaptive Metropolis algorithm using boreal forest site eddy covariance measurements, Nonlinear Processes in Geophysics, 23, 447–465, https://doi.org/10.5194/npg-23-447-2016, 2016.

Martino, L., Elvira, V., Luengo, D., and Corander, J.: An Adaptive Population Importance Sampler: Learning From Uncertainty., IEEE 30 Transactions on Signal Processing, 63, 4422–4437, https://doi.org/10.1109/TSP.2015.2440215, 2015.

Medlyn, B., Duursma, R., Eamus, D., Ellsworth, D., Prentice, I., Barton, C., Crous, K., De Angelis, P., Freeman, M., and Wingate, L.: Reconciling the optimal and empirical approaches to modelling stomatal conductance, Glob. Change Biol., 17, 2134–2144, https://doi.org/10.1111/j.1365-2486.2010.02375.x, 2011.

Medlyn, B., De Kauwe, M., and Duursma, R.: New developments in the effort to model ecosystems under water stress, New Phytol., 212, 35 5–7, https://doi.org/10.1111/nph.14082, 2016.

Muukkonen, P., Nevalainen, S., Lindgren, M., and Peltoniemi, M.: Spatial occurrence of drought-associated damages in Finnish boreal forests: results from forest condition monitoring and GIS analysis, Boreal Environ. Res., 20, 172–180, http://www.borenv.net/BER/pdfs/ber20/ber20-172.pdf, 2015.

Nemani, R., Keeling, C., Hashimoto, H., Jolly, W., Piper, S., Tucker, C., Myneni, R., and Running, S.: Climate-Driven Increases in Global Terrestrial Net Primary Production from 1982 to 1999, Science, 300, 1560–1563, https://doi.org/10.1126/science.1082750, 2003.

Nobel, P., ed.: Physicochemical and environmental plant physiology, Academic Press, https://doi.org/10.1016/B978-0-12-374143-1.X0001-4, 1999.

5 Owen, A. and Yi, Z.: Safe and Effective Importance Sampling, J. Am. Stat. Assoc., 95, 135–143, https://doi.org/10.2307/2669533, 2000.

Peylin, P., Bacour, C., MacBean, N., Leonard, S., Rayner, P., Kuppel, S., Koffi, E., Kane, A., Maignan, F., Chevallier, F., Ciais, P., and Prunet, P.: A new stepwise carbon cycle data assimilation system using multiple data streams to constrain the simulated land surface carbon cycle, Geoscientific Model Development, 9, 3321–3346, https://doi.org/10.5194/gmd-9-3321-2016, 2016.

Post, H., Vrugt, J.A. amd Fox, A., Vereecken, H., and Hendricks Franssen, H.-J.: Estimation of Community Land Model pa-
10 rameters for an improved assessment of net carbon fluxes at European sites, J. Geophys. Res.-Biogeosci., 122, 661–689, https://doi.org/10.1002/2015JG003297, 2017.

Powell, T., Galbraith, D., Christoffersen, B., Harper, A., Imbuzeiro, H., Rowland, L., Almeida, S., Brando, P., Lola da Costa, A., Costa, M., Naomi M. Levine, N., Malhi, Y., Saleska, S., Sotta, E., Williams, M., Meir, P., and Moorcroft, P.: Confronting model predictions of carbon fluxes with measurements of Amazon forests subjected to experimental drought, New Phytol., 200, 350–365, 10.1111/nph.12390, 2013.

15 Raddatz, T., Reick, C., Korr, W., Kattge, J., Roeckner, E., Schnur, R., Schnitzler, K.-G., Wetzel, P., and Jungclau, J.: Will the trop-
ical land biosphere dominate the climate–carbon cycle feedback during the twenty-first century?, Clim. Dynam., 29, 565–574, https://doi.org/10.1007/s00382-007-0247-8, 2007.

Rannik, U., Peltola, O., and Mammarella, I.: Random uncertainties of flux measurements by the eddy covariance technique, Atmos. Meas. Tech. Discuss., in review, 1–31, https://doi.org/10.5194/amt-2016-31, 2016.

20 Raoult, N.M., J. T. C. P. and Luke, C.: Land-surface parameter optimisation using data assimilation techniques: the adJULES system V1.0, Geosci. Model Dev., 9, 2833–2852, https://doi.org/10.5194/gmd-9-2833-2016, 2016.

Reick, C., Raddatz, T., Brovkin, V., and Gayler, V.: Representation of natural and anthropogenic land cover change in MPI-ESM, Journal of Advances in Modeling Earth Systems, 5, 1–24, https://doi.org/10.1002/jame.20022, 2013.

Richardson, A., Hollinger, D., Burba, G., Davis, K., Flanagan, L., Katul, G., Munger, J., Ricciutio, D., Stoy, P., Suyker, A., Verma, S., and
25 Wofsy, S.: A multi-site analysis of random error in tower-based measurements of carbon and energy fluxes, Agr. Forest Meteorol., 136, 1–18, https://doi.org/10.1016/j.agrformet.2006.01.007, 2006.

Richardson, A., Mahecha, M., Falge, E., Kattge, J., Moffat, A., Papale, D., Reichstein, M., Stauch, V., Braswell, B., Churkina, G., Kruijt, B., and Hollinger, D.: Statistical properties of random CO2 flux measurement uncertainty inferred from model residuals, Agr. Forest Meteorol., 148, 38–50, https://doi.org/10.1016/j.agrformet.2007.09.001, 2008.

30 Richardson, A., Anderson, R., Arain, M., Barr, A., Bohrer, G., Chen, G., Chen, J., Ciais, P., Davis, K., Desai, A., Dietze, M., Dragoni, D., Garrity, S., Gough, C., Grant, R., Hollinger, D., Margolis, H., Mccaughey, H., Migliavacca, M., Monson, R., Munger, J.W. Poulter, B., Raczka, B., Ricciuto, D., Sahoo, A., Schaefer, K., Tian, H., Vargas, R., Verbeeck, H., Xiao, J., and Xue, Y.: Terrestrial biosphere models need better representation of vegetation phenology: results from the North American Carbon Program Site Synthesis, Glob. Change Biol., 18, 566–584, https://doi.org/10.1111/j.1365-2486.2011.02562.x, 2012.

35 Roeckner, E., Bäuml, G., Bonaventura, L., Brokopf, R., Esch, M., Giorgetta, M., Hagemann, S., Kirchner, I., Kornblueh, L., Manzini, E., Rhodin, A., Schlese, U., Schulzweida, U., and Tompkins, A.: The atmospheric general circulation model ECHAM5. PART I: Model description, Max Planck Institute for Meteorology Report, 349, 1–127, http://www.mpimet.mpg.de/fileadmin/publikationen/Reports/max_scirep_349.pdf, 2003.

Schulze, E., Kelliher, F., Korner, C., Lloyd, J., and Leuning, R.: Relationships among Maximum Stomatal Conductance, Ecosystem Surface Conductance, Carbon Assimilation Rate, and Plant Nitrogen Nutrition: A Global Ecology Scaling Exercise, Annu. Rev. Ecol. Syst., 25, 629–662, http://www.jstor.org/stable/2097327, 1994.

Scott, D. W.: Multivariate Density Estimation and Visualization, http://EconPapers.repec.org/RePEc:zbw:caseps:200416, 2004.

5 Sellers, P.: Canopy reflectance, photosynthesis and transpiration, Int. J. Remote Sens., 6, 1335–1372, https://doi.org/10.1080/01431168508948283, 1985.

Singh, R., Reager, J., Miller, N., and Famiglietti, J.: Toward hyper-resolution land-surface modeling: The effects of fine-scale topography and soil texture on CLM4.0 simulations over the Southwestern U.S., Water Resour. Res., 51, 2648–2667, https://doi.org/10.1002/2014WR015686, 2015.

10 Tesfa, T., Li, H.-Y., Leung, L., Huang, M., Ke, Y., Sun, Y., and Liu, Y.: A subbasin-based framework to represent land surface processes in an Earth system model, Geosci. Model Dev., 7, 947–963, https://doi.org/10.5194/gmd-7-947-2014, 2014.

Thum, T., Aalto, T., Laurila, T., Aurela, M., Kolari, P., and Hari, P.: Parametrization of two photosynthesis models at the canopy scale in northern boreal Scots pine forest, Tellus, 59B, 874–890, https://doi.org/10.1111/j.1600-0889.2007.00305.x, 2007.

Trudinger, C., Raupach, M., Rayner, P., Kattge, J., Liu, Q., Pak, B., Reichstein, M., Renzullo, L., Richardson, A., Roxburgh, S., Styles, J.,
15 Wang, Y., Briggs, P., Barrett, D., and Nikolova, S.: OptIC project: An intercomparison of optimization techniques for parameter estimation in terrestrial biogeochemical models, J. Geophys. Res-Biogeo., 112, G02 027, https://doi.org/10.1029/2006JG000367, 2007.

Ueyama, M., Tahara, N., Iwata, H., Euskirchen, E., Ikawa, H., Kobyashi, H., Nagano, H., Nakai, T., and Harazono, Y.: Optimization if a biochemical model with eddy covariance measurements in black spruce forests of Alaska for estimating CO_2 fertilization effects, Agr. Forest Meteorol., 222, 98–111, https://doi.org/10.1016/j.agrformet.2016.03.007, 2016.

20 Veach, E. and Guibas, L.: Optimally Combining Sampling Techniques for Monte Carlo Rendering, SIGGRAPH 1995 Proceedings, pp. 419–428, https://doi.org/10.1145/218380.218498, 1995.

Wang, K.-Y.: Canopy CO_2 exchange of Scots pine and its seasonal variation after four-year exposure to elevated CO_2 and temperature, Agr. Forest Meteorol., 82, 1–27, https://doi.org/10.1016/0168-1923(96)02342-8, 1996.

Xu, Z., Shimizu, H., Yagasaki, Y., Ito, S., Zheng, Y., and Zhou, G.: Interactive Effects of Elevated CO_2, Drought, and Warming on Plants, J.
25 Plant Growth Regul., 32, 692–707, https://doi.org/10.1007/s00344-013-9337-5, 2013.

Zhou, S., Duursma, R., Medlyn, B., Kelly, J., and Prentice, I.: How should we model plant responses to drought? An analysis of stomatal and non-stomatal responses to water stress, Agric. Forest Meteorol., 182–183, 204–214, https://doi.org/10.1016/j.agrformet.2013.05.009, 2013.
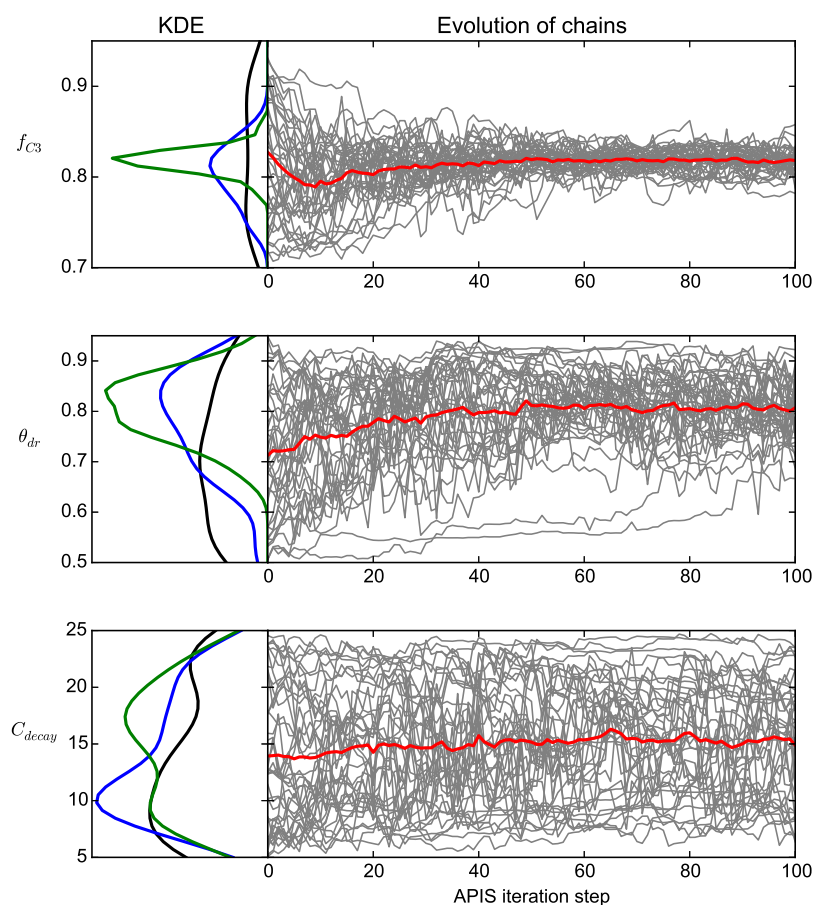
Figure 1. Examples of the evolution of the APIS algorithm from the Bethy calibration. The right panel shows how the location parameters (gray) of the parameter proposal distributions and the global estimate of the parameter expected value (red) are adapted throughout the process. The left panel is the kernel density estimate of the spread of the location parameters at the start of the process (black), after 20 iterations (blue) and after 100 iterations (green).
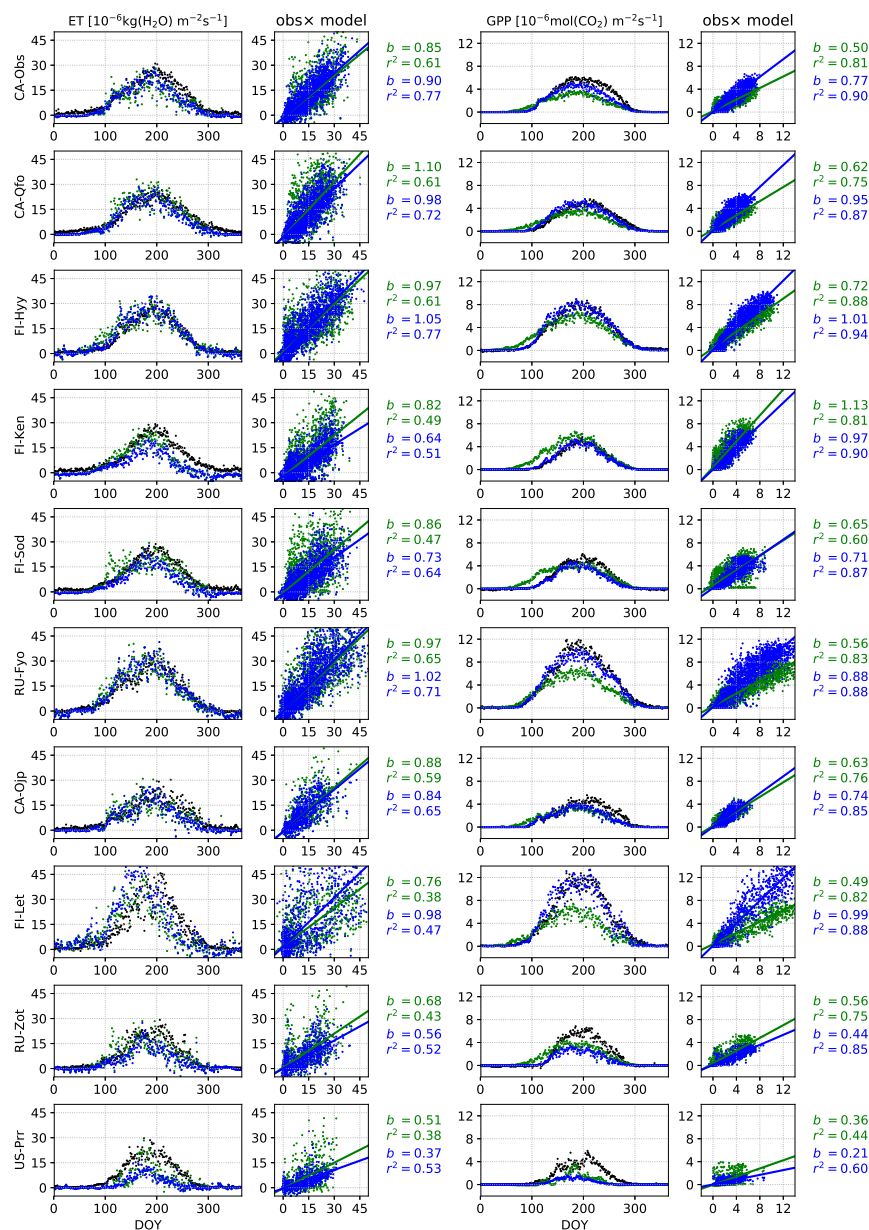
Figure 2. Validation period average annual cycles of evapotranspiration and gross primary production; observations (black) and the model using the Bethy stomatal conductance formulation with default (green) and optimised (blue) parametrisation. Also presented are daily model values cross plotted against observations with corresponding slope of the regression line (b) and the coefficient of determination (r^2).
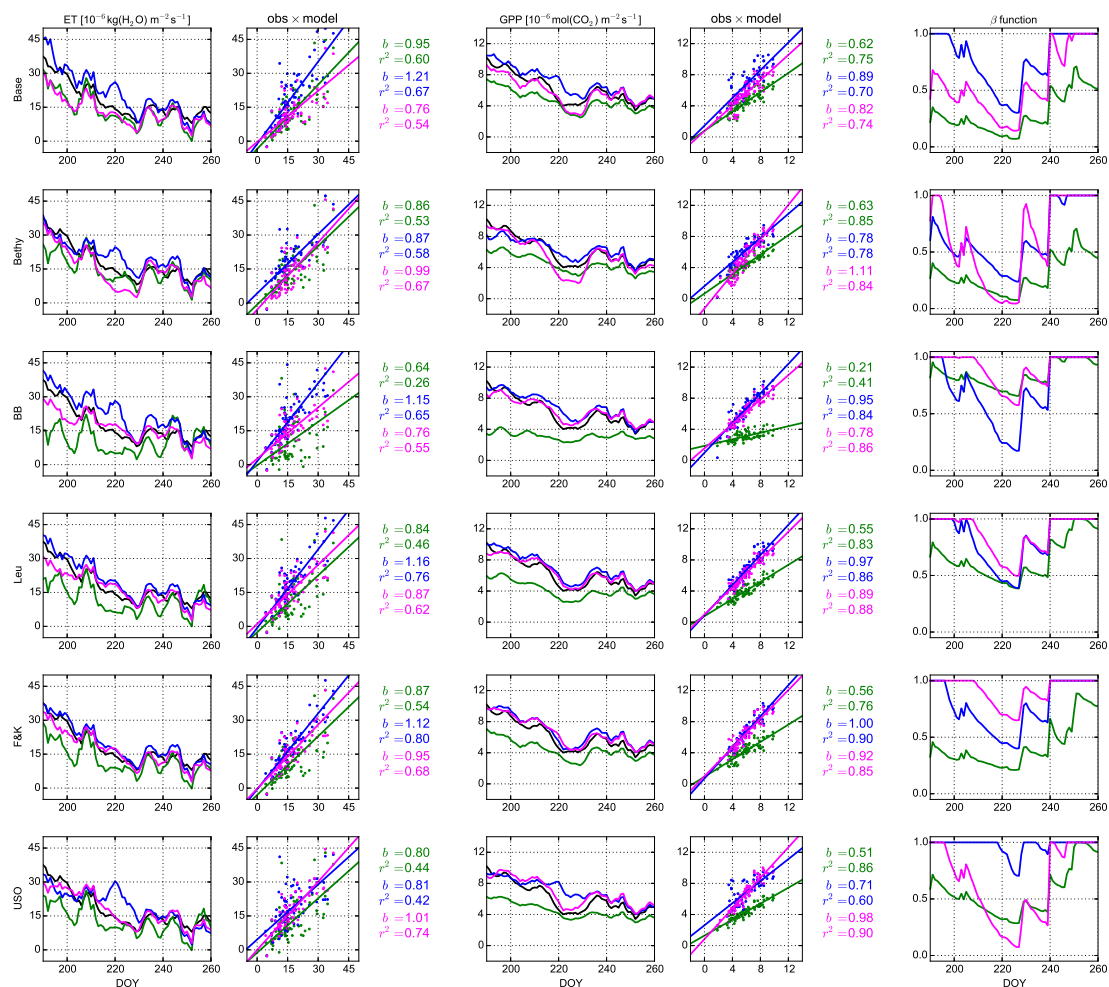
Figure 3. Hyytiälä site drought in summer 2006. The time series for evapotranspiration and gross primary production are 5-day running averages and for β-function daily values. The observations are plotted in black and the model with default parametrisation in green, calibration period optimisation in blue and the dry year optimisation in magenta.
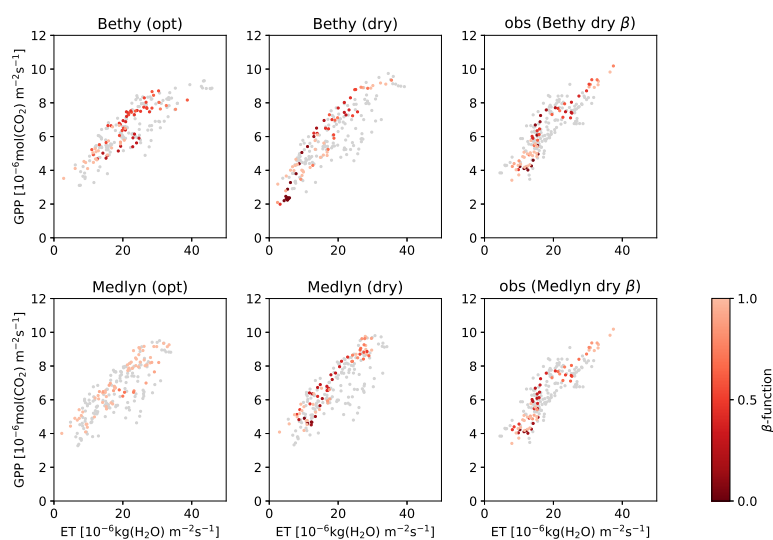
Figure 4. Hyytiälä site water use efficiency for the Bethy and USO formulations. Scatter plotted are the dry period 5-day running averages of ET and GPP, coloured by the intensity of the drought (β-function). The left column depicts the model with the more generally optimised parameter values, the middle column with the drought optimisation and the right column presents the corresponding observations, coloured by the same intensity as in the middle column. The grey points are from the corresponding time in the two previous years.